

1 Stream water sourcing from high elevation snowpack inferred from 2 stable isotopes of water: A novel application of *d-excess* values

3 Matthias Sprenger^{1*}, Rosemary W.H. Carroll², David Marchetti³, Carleton Bern⁴, Harsh Beria⁵, Wendy Brown⁶,
4 Alexander Newman⁶, Curtis Beutler⁶, Kenneth H. Williams^{1,6}

5 ¹Lawrence Berkeley National Laboratory, Berkeley, CA, USA

6 ²Desert Research Institute, Reno, NV, USA

7 ³Western Colorado University, Gunnison, CO, USA

8 ⁴U.S. Geological Survey, Denver, CO, USA

9 ⁵Department of Environmental Systems Science, ETH Zurich, Zurich, Switzerland

10 ⁶Rocky Mountain Biological Laboratory, Crested Butte, CO, USA

11 *Corresponding author: msprenger@lbl.gov

12
13 **Abstract.** About 80% of the precipitation in the Colorado River's headwaters is snow, and the resulting snowmelt-
14 driven hydrograph is a crucial water source for about 40 million people. Snowmelt from alpine and subalpine
15 snowpack contributes substantially to groundwater recharge and river flow. However, the dynamics of snowmelt
16 progression are not well understood because observations of the high elevation snowpack are difficult due to
17 challenging access in complex mountainous terrain as well as the cost- and labor-intensity of currently available
18 methods. We present a novel approach to infer the processes and dynamics of high elevation snowmelt contributions
19 predicated upon stable hydrogen and oxygen isotope ratios observed in stream flow-discharge. We show that
20 deuterium-excess (*d-excess*) values of stream water can-should serve as a comparatively cost-effective proxy for a
21 catchment integrated signal of high elevation snow melt contributions to catchment runoff.

22 We sampled stable hydrogen and oxygen isotope ratios of the precipitation, snowpack, and stream water in the East
23 River, a headwater catchment of the Colorado River and the stream water of larger catchments at sites on the Gunnison
24 River and Colorado River.

25 The *d-excess* of snowpack increased with elevation; the upper subalpine and alpine snowpack (>3200 m) ~~and~~ had a
26 substantially higher *d-excess* compared to lower elevations (<3200 m) in the study area. The *d-excess* values of stream
27 water reflected this because *d-excess* values increased as the higher elevation snowpack contributed more to stream
28 water generation later in the snowmelt/runoff season. Endmember mixing analyses based on the *d-excess* data showed
29 that the share of high elevation snowmelt contributions within the snowmelt hydrograph was on average 44% and
30 generally increased during melt period progression, up to 70%. The observed pattern was consistent during six years
31 for the East River, and a similar relation was found for the larger catchments on the Gunnison and Colorado Rivers.

32 High elevation snowpack contributions were found to be higher for years with lower snowpack and warmer spring
33 temperatures. Thus, we conclude that the *d-excess* of stream water is a viable proxy to observe changes in high
34 elevation snowmelt contributions in catchments at various scales. Inter-catchment comparisons and temporal trends
35 of the *d-excess* of stream water could therefore serve as a catchment-integrated measure to monitor if mountain
36 systems ~~increasingly~~ rely more on high elevation water inputs during snow drought compared to years of average
37 snowpack depths.

38 1 Introduction

39 The snowpack in mountainous regions provides a crucial water source for the ecosystems and human activities
40 downstream (Immerzeel et al., 2020). In the alpine and subalpine headwaters of semi-arid regions where the summer
41 precipitation contribution to streamflow is usually relatively low, as in the southwestern United States, snowmelt
42 sustains streamflow during much of the growing season when water demands are higher. The Colorado River plays a
43 special role in the hydrology of the southwestern United States because its headwaters in the Rocky Mountains support
44 the water supply for about 40 million people, agriculture, industry and power generation (Bureau of Reclamation,
45 2012). The snowmelt from high elevation upper subalpine and alpine regions of the mountainous headwaters of the
46 Colorado River was shown to be particularly important for ~~the~~ groundwater recharge and sustaining river flow (Carroll
47 et al., 2019). However, observed (Faybishenko et al., 2022; Hoerling et al., 2019) and projected (Bennett and Talsma,
48 2021) increases in air temperatures in the headwaters of the Colorado River can lead to a decrease of the snow-to-rain
49 ratio during the coming decades (Hammond et al., 2023). Therefore, ~~if carbon emissions are not reduced,~~ the
50 mountainous catchments in the Colorado River could likely transition towards low-to-no snow conditions during the
51 second half of this century (Siirila-Woodburn et al., 2021). ~~Because we already observe~~ In fact, a general trend towards
52 lower snow packs and earlier snowmelt in the western United States is already observed (Musselman et al., 2021), ~~it~~
53 ~~is crucial to better understand the role of high elevation snowpack in streamflow dynamics~~. However, the tools needed
54 to observe high elevation snowmelt processes are either missing (e.g. point observations), too coarse a resolution (e.g.
55 satellite), or expensive to obtain (e.g. airborne lidar (Light Detection and Ranging) techniques, numerical models),
56 which is why we investigate the use of a stable isotope-based method that can help assess upper subalpine and alpine
57 snowmelt contributions to streamflow.

58 Snowpack assessments and snowmelt dynamics are usually monitored with point observations like the U.S. Natural
59 Resource Conservation Service's (NRCS) SNOW TELemetry (SNOTEL) network (NWCC, 2023). However, the
60 highest elevations in the western United States are not covered by this network (max. elevation 3543 m a.s.l.), despite
61 this area harboring the largest snow water equivalent (SWE) and most surface water input volumes per square meter
62 (Hammond et al., 2023). Therefore, ~~although while~~ the measured snow pack at SNOTEL sites will indicate melt-out,
63 there remains substantial snow cover in the alpine regions past the SNOTEL indicated melt-out dates (Dozier et al.,
64 2016). To obtain a spatial representation of the SWE from the SNOTEL point measurements, regression analyses with
65 physiographic variables (e.g., elevation, slope, aspect) are commonly used (Fassnacht et al., 2003). Heterogeneity of
66 snowfall accumulation and redistribution of snow (Freudiger et al., 2017) in complex mountainous terrain makes such
67 interpolation and extrapolation efforts difficult (Dozier et al., 2016). Adding information about the previous year's

68 snow cover distribution from satellite data was shown to improve the reconstruction of SWE across the complex
69 mountainous terrain of the Upper Colorado River Basin (Schneider and Molotch, 2016). However, maps of snowpack
70 distribution from airborne snow observatory (ASO) based on airborne light-detectionlidar (Painter et al., 2016) are
71 costly and therefore may not be applicable across multiple mountainous catchments and/or during several years.

72 In addition to the high costs and labor intensity of the currently available methods to study high elevation snowmelt
73 dynamics, these approaches are generally limited to hydrometric data and do not include any tracer information. Beria
74 et al. (2018) outlined multiple ways how stable hydrogen and oxygen isotopes of water ($\delta^2\text{H}$ and $\delta^{18}\text{O}$) can provide
75 valuable insights into snow hydrological processes. Because hydrogen and oxygen isotopes comprise the water
76 molecule, $\delta^2\text{H}$ and $\delta^{18}\text{O}$ signatures are ideal tracers to track fluxes in the water cycle (Kendall and McDonnell, 1998).

77 Stable hydrogen and oxygen isotopes of water have long been used to infer snowmelt contributions to stream water
78 (e.g., Rodhe, 1981). However, because groundwater recharge is predominantly by snowmelt in snow dominated semi-
79 arid environments (Sprenger et al., 2022), the isotopic difference between snowmelt newly contributing to the stream
80 discharge and the groundwater dominated stream flow during baseflow makes mixing model applications unfeasible
81 in such environments. We therefore explore the applicability of the *d-excess* value as an alternative tracer. This metric
82 is based on ~~the relationship~~ between the ~~relative stable~~ hydrogen and oxygen isotope ratios of water systems, which
83 was identified by Craig (1961a) as

$$84 \quad \delta^2H = 8 \times \delta^{18}O + 10 \quad (1)$$

85 and who characterized this ~~relationship~~ as indicative of “waters which have not undergone excessive
86 evapotranspiration.” Dansgaard (1964) defined the concept of deuterium-excess, or *d-excess*, as

$$87 \quad d\text{-excess} = \delta^2H - 8 \times \delta^{18}O \quad (2)$$

88 which can be interpreted as an index of non-equilibrium in the simple condensation - evaporation of global
89 precipitation. This formulation has been useful for screening isotopic results from water samples: values of *d-excess*
90 between 10 and 11 are effectively the intercept in Craig’s proposed ~~relationship~~ and indicate quasi-stable conditions
91 at a relative humidity of ~85% (Dansgaard, 1964; Gat, 2000). Here, we test two hypotheses to examine how *d-excess*
92 data from stream water samples are related to high elevation snowmelt contributions to the catchment runoff during
93 the snowmelt periods. First, we hypothesize that *d-excess* values in stream water during the snowmelt hydrograph
94 reflect the changing dominance of snowmelt contributions through time from lower to higher elevations. Second, we
95 test if these patterns of *d-excess* of stream water are detectable across ranges in drainage area, thus increasing their
96 broader applicability.

97

98 **2 Methods**

99 **2.1 Study sites and data**

100 Our study is situated in the headwaters region of the Upper Colorado River (Figure 1) with a focus on an East River
101 subcatchment (85 km²) as defined by the gaging and sampling station at the Pumphouse location (38.922447, -
102 106.950828) near Mount Crested Butte, CO. The Pumphouse subcatchment has a large elevation gradient from about
103 2700 to 4100 m (Figure 1) and is predominantly underlain by Paleozoic and Mesozoic sedimentary rocks, including
104 Mancos Shale that covers 44% of the catchment area, and localized intrusive igneous rocks like granodiorite (Gaskill
105 et al., 1991). The Varying dominance of vegetation with elevation define four ecozones in the catchment: is dominated
106 by shrubs, grasses, and forbs #dominate the montane (<2800 m elevation, 2% of catchment area) zone, aspen and
107 conifers dominate in the lower subalpine (2800 to 3200 m, 34% of the catchment area) region, and conifers dominate
108 in the upper subalpine (3200 to 3500 m, 32% of the catchment area) regions. In the alpine region (>3500 m, 31% of
109 the catchment area), shrubs are dominant until 3800 m, above which land is mostly barren (Carroll, Deems, Sprenger,
110 et al., 2022). Meadows are distributed across the catchment, but take up a relatively small share of the total area above
111 the montane. The climate is dominated by cold winters with substantial snow cover and snowpack accumulation that
112 constitutes about 80% of the total annual precipitation (Carroll, Deems, Sprenger, et al., 2022). There is a consistent
113 snowpack cover in the subalpine and alpine region with no mid-winter melt. In the montane region melt is very limited
114 (<10 mm/day) prior to early March (Carroll et al., 2022a). The dominant moisture source of winter precipitation in
115 the study region is the northeastern Pacific and snowfall occurs predominantly from northwestern frontal storms
116 (Marchetti and Marchetti, 2019). Summers are relatively warm and dry with monsoonal rain that accounts for 20% of
117 the annual precipitation. The snowpack depth is generally greater and snowmelt timing is later with increasing
118 elevation across the catchment (Carroll et al., 2022a). The catchment hydrograph is dominated by the snowmelt pulse
119 with an onset in April, a pronounced peak during June and a subsequent snowmelt recession interspersed with smaller
120 peaks driven by monsoon rainfall events. Between September and March, the catchment streamflow is generally
121 limited to base flow (Carroll et al., 2020). The East River has been intensely instrumented and studied since 2015;
122 more details are provided in Hubbard et al. (2018).

123 In addition to the East River, we also sampled the Upper Gunnison River near Gunnison, CO, about 50 km downstream
124 from Mount Crested Butte. This catchment is defined by the USGS streamgage #09114500 (38.54193567, -
125 106.9497661) and has a drainage area of 2,618 km². A third basin was included, which is defined by the USGS
126 streamgage # 09095500 (39.2391463 -108.2661946) of the main stem of the Colorado River near Cameo, CO. Its
127 drainage area is of 20,683 km² (USGS, 2023). Hereafter, these two basins locations are referred to as Gunnison and
128 Cameo, respectively, and their catchment areas are shown in Figure 1.

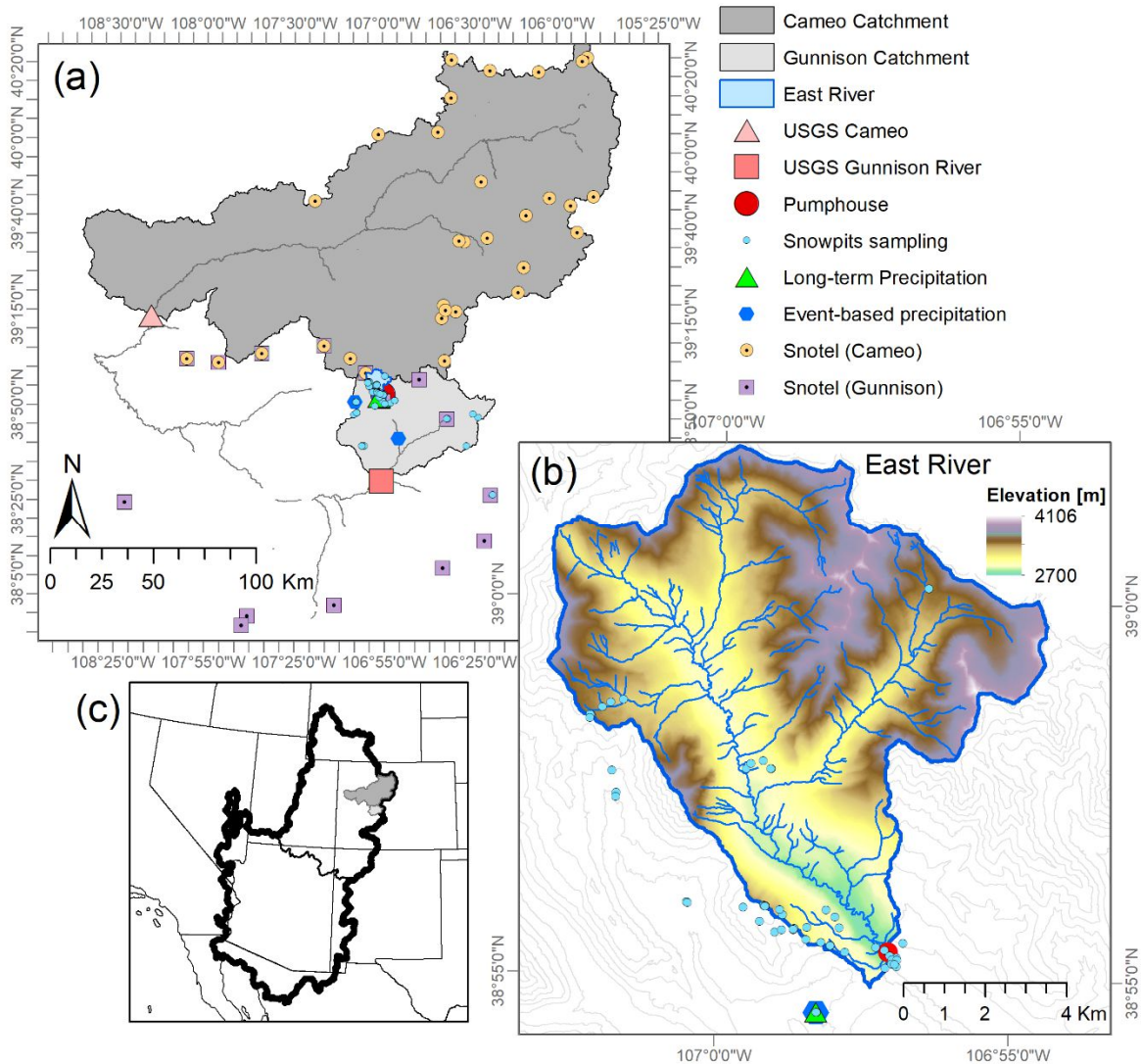
129 Within the Gunnison River Basin, there are 15 SNOTEL sites located at elevations ranging between 2674 and 3523
130 m providing snow water equivalent (SWE) observations (Suppl. Table 1). Across these SNOTEL sites, elevation was
131 not a good predictor for the maximum snowpack depth (Suppl. Fig. 1). For the Colorado River at Cameo, we chose
132 the 31 SNOTEL sites in the Colorado Headwaters ranging between 2610 and 3452 m (NWCC, 2023) (Figure 1).

133 We sampled snowpack between 2016 and 2019 across a gradient spanning 1324 m in elevation (from 2347 to 3671
134 m) in the Gunnison catchment (Figure 1a&b). The snowpack sampling generally took place between early February
135 and late May with 80% of all samples taken +/- 30 days of April 1st, which is often assumed to be the timing of peak

136 SWE. A total of 53 snow pits were dug in flat areas with samples collected in duplicate at 10-cm depth increments to
137 tabulate snow density, temperature, and stable isotope ratios. Bulk snowpack isotopic content represents the SWE-
138 weighted composite value across the entire snow column (Carroll et al., 2022b). Precipitation was first sampled on an
139 event basis via a collector from 2014 to 2017 in Mount Crested Butte at 2885 m (“long-term Precipitation” in Figure
140 1), and the sampling procedure was outlined in Carroll et al. (2022b). Since 2020, we sampled the precipitation on an
141 approximate event basis at the locations Estess (2513 m), Mount Crested Butte (2885 m), and Irwin Barn (3181 m)-
142 (“Event-based precipitation” in Figure 1). We sampled stream water from the East River at the Pumphouse location
143 from 2014 to 2022 on daily to fortnightly frequency (“Pumphouse in Figure 1). There was a gap of sampling in April
144 2018; and therefore, 2018 was excluded from the present analyses. The East River stable isotope data are published
145 in Williams (2023). Sampling at the Gunnison River was done between March 2020 and December 2021 on a weekly
146 basis with occasional higher (3 days) or lower (15 days) frequency. At Cameo, stream water sampling occurred at
147 weekly to fortnightly frequency in 2021 and 2022.

148 All water samples were measured for stable hydrogen and oxygen isotopes using a Cavity Ring-Down Spectroscopy
149 (Picarro L2130-i). We report isotope ratios as $\delta^{18}\text{O}$ and $\delta^2\text{H}$ values expressed relative to the Vienna Standard Mean
150 Ocean Water (Craig, 1961b).

151



152

153 **Figure 1 (a)** Locations of streamgages and water sampling of the Colorado River near Cameo and the Gunnison River ~~in~~
 154 ~~near~~ Gunnison ~~(black markers)~~ and the river's catchment area (grey). Locations of event-based precipitation sampling
 155 (blue markers), SNOTEL stations in the Colorado ~~River~~ (light blue) and Gunnison ~~River~~ (light purple) areas. East River
 156 catchment area (blue outline) as defined by Pumphouse gaging and sampling location (red circle) located within the
 157 Gunnison river catchment also shown. (b) Area and elevation of the East River catchment with the streamgage and water
 158 sampling location at Pumphouse (red marker) and long-term precipitation sampling site (cyan triangle). (c) Locations of
 159 the catchments defined by the stream gages near Cameo and Gunnison (light grey) in the Colorado River Basin (thick black
 160 line).

161 2.2 Data analyses

162 We calculated the deuterium excess value (short "*d-excess*") for all water samples as defined by equation (2).

163 ~~While it was shown that the *d-excess* of precipitation is on average about 11.27% on a global scale (Rozanski et al.,~~
 164 ~~1993), for snowpacks, the *d-excess* values were found to increase with elevation (Froehlich et al., 2008; Tappa et al.,~~
 165 ~~2016) due to increased evaporative fractionation from lower elevation snowpacks which are re-condensed at higher~~
 166 ~~elevations (Lambán et al., 2015). Because ~~t~~he slope of the local meteorologic water line ~~is~~, observed to be 7.4 (Carroll~~

167 et al., 2022b) near Mt Crested Butte and 7.2 at the lower elevation Gunnison site (Marchetti and Marchetti, 2019),
168 which does not deviate much from the slope of 8 of the global meteorologic water line that defines the *d-excess* (see
169 Suppl. Fig. 2), ~~we decided to use the *d-excess* rather than *le-excess* (Landwehr and Coplen, 2006). We used linear~~
170 ~~correlation analyses to describe various relation and provide Pearson (r) coefficients.~~ For significant linear Pearson
171 correlations ($p < 0.05$), we added linear regression lines to the plots.

172 We used the SNOTEL data to compute the fraction of peak-maximum SWE through time for each water year (a value
173 of one equals maximum SWE and zero indicates the snowpack is melted). Because SNOTEL SWE data only reflects
174 conditions at the stations, we used spatially explicit energy balance snowmelt simulations, as published by Carroll et
175 al. (2022a), that were informed by the spatial variation in SWE as observed by flights of the airborne snow observatory
176 (ASO). For each water year with snowmelt simulations available, we calculated the cumulative difference through
177 time between the simulated snowmelt for the montane and alpine elevation bands in the East River, given as millimeter
178 (mm) SWE. In this case, a value of zero indicated equal snowmelt volumes from the montane and alpine snowpack,
179 whereas positive values show that alpine snowmelt exceeded montane snowmelt.

180 We defined the snowmelt period in the East River catchment based on the hydrograph at the Pumphouse streamgage
181 to be the time between day 200 and 300 of the water year. This period is between Mid-April to late July, because the
182 water year starts on October 1st. For the snowmelt period, we applied for each day with a stream water sample the
183 used the Bayesian mixing framework model HydroMix, developed by Beria et al. (2020), to estimate the contribution
184 temporal dynamics of the share of high elevation snowmelt in to the streamflow during the snowmelt period, which
185 occurred between day 200 to 300 of the water year (water year starts on October 1st). HydroMix uses tracer data of
186 the end-members and the mixture to estimate the probability distribution function (pdf) of the mixing ratio, defined as
187 fractional contribution of end-members to the mixture:

$$188 \rho S_1 + (1 - \rho) S_2 = M, \quad (3)$$

189 where M is the tracer concentration in the mixture, S_1 and S_2 are tracer concentrations in the two sources, and ρ is the
190 fractional contribution of S_1 to mixture M .

191 In typical Bayesian mixing analysis, pdfs are fitted to tracer concentrations in different end-members and the mixture,
192 and the pdf of the mixing ratio is estimated using standard Bayesian inference principles. This requires a large tracer
193 dataset to ensure a robust fit to tracers of the end-members and the mixture, which is often not available. HydroMix
194 adopts a bootstrap approach, using all possible combinations of end-member tracer measurements and formulating a
195 likelihood function based on an assumed pdf of the underlying error function, which is the difference between
196 simulated and observed mixture concentration. By using all available combinations of end-member tracer
197 measurements, HydroMix builds an empirical pdf while optimizing the likelihood function. This approach has been
198 shown to work both theoretically and in real-case scenarios (Beria et al., 2020).

199 The two end members (S_1 and S_2) were defined as the *d-excess* of the snowpack from the upper subalpine and alpine
200 snowpack (>3200 m, n=31, defined as “high elevation”) and lower subalpine and montane area (<3200 m, n=60),
201 respectively. We report the mean fraction of high elevation snowmelt in each water sample (M) with standard

202 deviations based on the distribution of the two endmembers as described in Beria et al. (2020). We further report the
203 seasonal ~~flow weighted mean~~~~average and maximum~~ share of high elevation snowpack in the stream samples. We
204 compared the HydroMix results with MixSIAR (Stock et al., 2018) calculations and found ~~with~~ both methods
205 ~~produced~~ very similar results. A ~~multiple~~ **Multiple** linear regression was used to explore the predictability of the
206 ~~mean~~~~maximum~~ share of high elevation snowmelt during the different years as a function of the ~~average~~ maximum SWE
207 (~~SWE_{Max}~~) and the mean air temperature (~~T_{air}~~ of measurements) at the Gunnison SNOTEL sites (NWCC, 2023) during
208 the snowmelt period.

209 **3 Results**

210 **3.1 The *d*-excess of stream water increased with high elevation snowmelt contributions**

211 Our snowpack sampling campaigns along a 1324 m elevation gradient showed that the average (\pm SD) *d*-excess value
212 of the high elevation (>3200 m) snowpack was 13.8 (\pm 1.6) ‰ and thus significantly higher than for the lower elevation
213 snowpack 10.7 (\pm 1.8) ‰ (Figure 2c). The *d*-excess of the lower elevation snowpack was not significantly different
214 from groundwater (10.5 \pm 1.0 ‰, Figure 2c) nor from the *d*-excess of summer rainfall (Suppl. Fig. 3). We further
215 observed a strong and temporally consistent (generally $r > 0.63$ and $p < 0.05$ for the four individual years) increase in
216 *d*-excess of the snowpack with elevation (Figure 2b). The *d*-excess lapse rate of the snowpack ~~was~~ +0.52 ‰/100 m,
217 leading to 12.9 ‰ to 14.4 ‰ and 14.4 ‰ to 17.6 ‰ for the *d*-excess of the snowpack in the upper subalpine and alpine
218 region, respectively. Lapse rates for the snowpack were not seen in $\delta^{18}\text{O}$ (Figure 2b) or $\delta^2\text{H}$ (data not shown). The
219 precipitation sampled via collectors across the 667 m elevation gradient from the event-based sampler also showed a
220 relation between average *d*-excess and elevation for the samples collected weekly to fortnightly between November
221 and April during water years 2021 and 2022 (Suppl. Fig. 4). These samples reflect a *d*-excess lapse rate for winter
222 precipitation of +0.7 ‰/100 m, which was slightly higher than snowpack, though the elevation range for the
223 precipitation sampler was lower. There was generally a large variability of SWE dynamics across the SNOTEL sites
224 in the Gunnison catchment (Figure 3a), and this variation among the sites did not result from elevation differences
225 (Suppl. Fig. 1).

226 The hydrograph of the snowmelt period had peak streamflow during May and June, a recession towards August and
227 lowest flows between September and March (Figure 3a). This pattern was consistent during the seven water years, but
228 years with lower SWE resulted in lower peak flows, as expected (Suppl. Fig. 5).

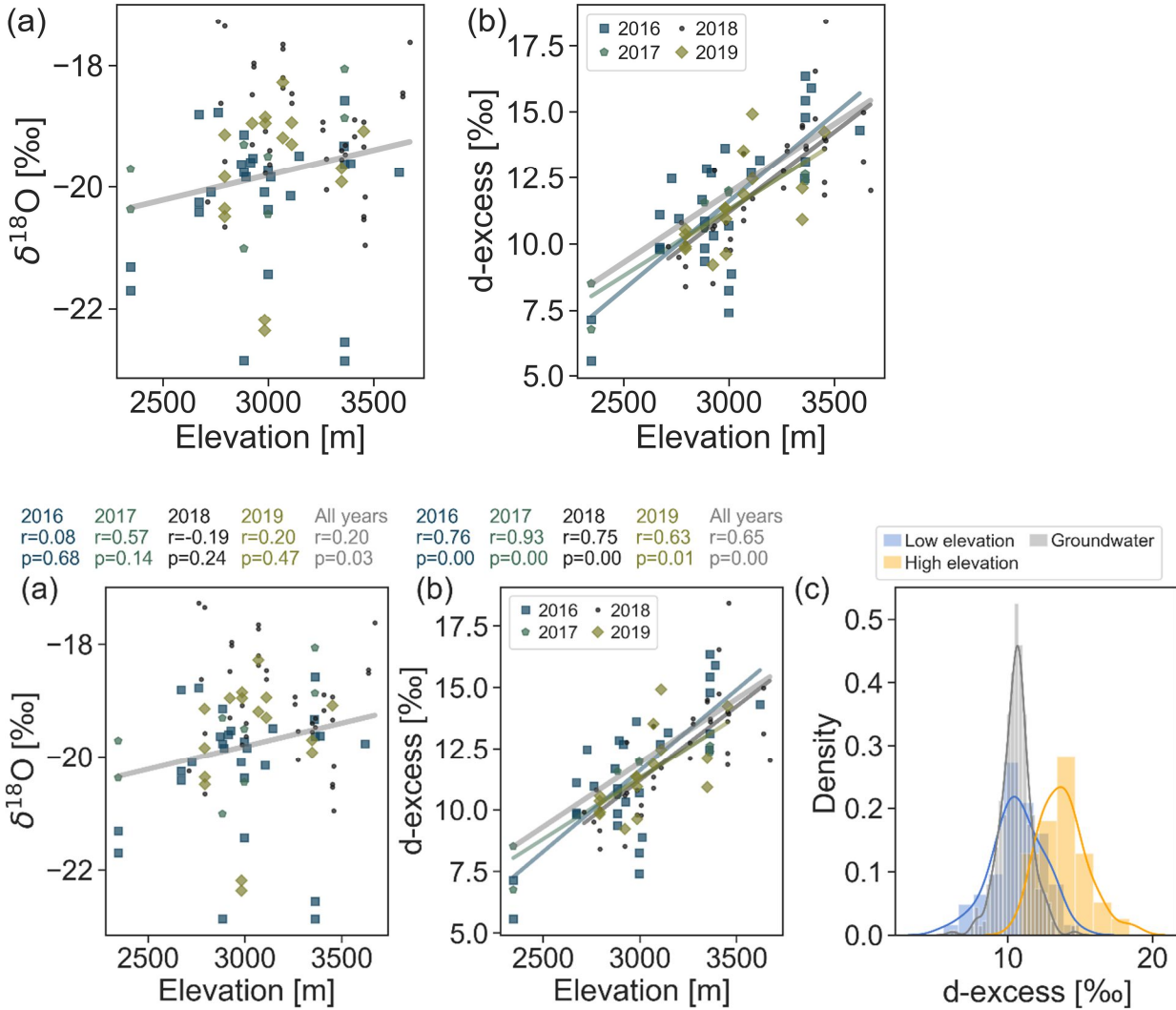
229 The stream water $\delta^{18}\text{O}$ dynamics reflected the seasonality of precipitation inputs, from having lower values (depleted
230 in ^{18}O) during peak flow and trending towards higher values (enriched in ^{18}O) during summer and early fall due to
231 greater fractional contributions from base flow and rainfall contributions that had higher $\delta^{18}\text{O}$ values compared to the
232 snowfall. Due to the strong difference in $\delta^{18}\text{O}$ values of rain and snowfall (see discussion in Sprenger et al., 2022), the
233 $\delta^{18}\text{O}$ of stream water decreased during the low flows in winter due to a higher fraction of groundwater sourced from
234 snowmelt vs. rain in the catchment runoff (orange points and line in Figure 3b). The $\delta^{18}\text{O}$ of snowmelt stream water
235 reached a minimum in June during maximum snowmelt contribution, after which the snowpack ceased to exist and
236 $\delta^{18}\text{O}$ of stream water increased throughout the summer with recession to base flow and monsoonal rainfall.

237 We found that over the study period, the timing of the peak stream flow could be explained by the timing of the most
238 intense snowmelt (i.e., slope of SWE in Figure 3) and the timing of the complete melt out at the higher (>3200 m)
239 SNOTEL stations (r=0.83 and r=0.79, respectively).

240 The *d-excess* values of stream water did not show a strong seasonal dynamic, but in general, *d-excess* values mainly
241 increased during the snowmelt season and subsequently dropped again during the summer (red points and line in
242 Figure 3b). The increase of *d-excess* of stream water was not due to ~~the~~ rainfall input because there was no seasonal
243 trend in *d-excess* of rainfall (Suppl. Fig. 3). Instead, *d-excess* of stream water resulted from melting snowpack at higher
244 elevations due to snowmelt progression, as evidenced by the SNOTEL SWE data, that resulted in increases in *d-excess*
245 of stream water consistently for each of the investigated years (Figure 4a). The hypothesis that this increase in *d-*
246 *excess* of stream water resulted from high elevation snowmelt contributions is supported by its relation with simulated
247 snowmelt differences between alpine and montane snowmelt volumes through time (Figure 4b). When the high
248 elevation snowmelt volumes became increasingly larger than the low elevation snowmelt, *d-excess* of stream water
249 increased consistently. Annual average snowmelt from alpine regions (1075 m³/s) was more than double than
250 snowmelt from montane regions (520 m³/s), despite the area of the prior (111 km²) being smaller than the latter (143
251 km²) in Carroll (2022a)'s modeling domain of the East River. Notably, Figure 4b also shows that ~~stream water~~ *d-*
252 *excess* values of stream water were highest for years with largest differences between alpine and montane snowpack
253 (2017 and 2019).

254 Our *d-excess*-based endmember mixing analyses revealed that 41 to 57% of the flow in the East River during the
255 snowmelt period stemmed from high elevation snowpack (Figure 5 ~~left~~). Periods when there were ~~an~~ increases in
256 the fraction of high elevation snowmelt contributions tend to be later in the snowmelt hydrograph and coincided with
257 periods of runoff intensification (Suppl. Fig. 6 ~~Figure 5, right~~). During peak alpine snowmelt contributions, about two-
258 thirds of the East River flow stemmed from the high elevation snowpack. There was a general trend that the annual
259 maximum-mean high elevation snowpack contributions were higher in water years with lower maximum SWE
260 observed at the SNOTEL sites across Gunnison county (Suppl. Fig. 7a, r=-0.51, p=0.24). However, the relatively
261 warm snowmelt period of 2017, following a winter with deep snowpack, resulted in relatively large high elevation
262 snowmelt contributions and thus did not follow that trend (Suppl. Fig. 7b, r=0.25, p=0.58). Because of this observation,
263 we included in addition to maximum SWE the average air temperature measured at the SNOTEL sites during the
264 snowmelt period as a second variable in a multiple regression analysis. The regression equation
265 mean high elevation snowmelt contribution = -37.03*T_{air} - 0.73*SWE_{max} + 0.089*T_{air}*SWE_{Max} + 350.74 (4)
266 explained 66% of the interannual variation of the maximum-mean high elevation snowmelt contribution, and all
267 variables had significance levels of <0.1. Our results therefore indicate that the snowpack at the highest elevation ~~can~~
268 ~~be~~ was most re important for runoff generation in low-snow years and relatively high air temperature ~~and~~ and years
269 with a deep snowpack and when the relatively low air temperature is higher (Figure 6). We also tested the streamflow
270 volumes during the snowmelt period as a variable, but did not include it, because of its strong correlation with SWE_{max}
271 (r=0.84, p=0.018).

2016	2017	2018	2019	All years	2016	2017	2018	2019	All years
r=0.08	r=0.57	r=-0.19	r=0.20	r=0.20	r=0.76	r=0.93	r=0.75	r=0.63	r=0.65
p=0.68	p=0.14	p=0.24	p=0.47	p=0.03	p=0.00	p=0.00	p=0.00	p=0.01	p=0.00
b=0.0003	b=0.0014	b=-0.0007	b=0.0011	b=0.0008	b=0.0066	b=0.0050	b=0.0061	b=0.0051	b=0.0052
a=-21.09	a=-23.71	a=-16.93	a=-23.04	a=-22.28	a=-8.25	a=-3.67	a=-7.01	a=-3.98	a=-3.78

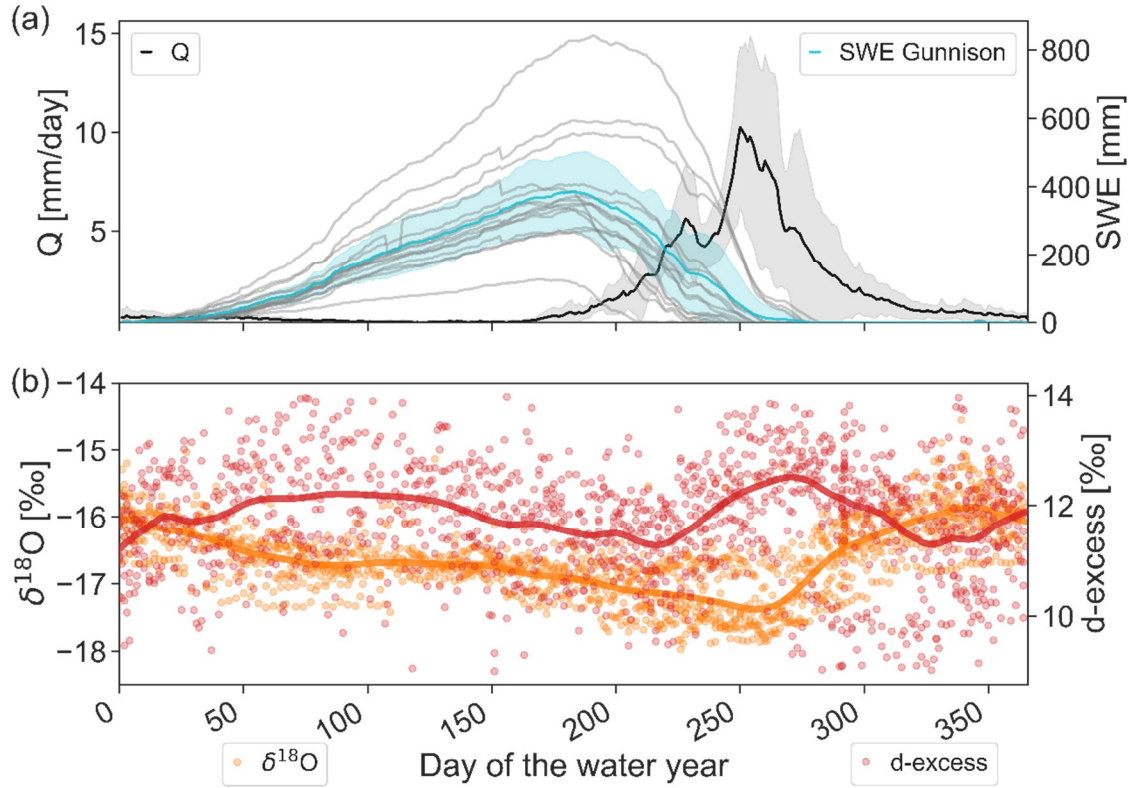


273

274

275 **Figure 2** The $\delta^{18}\text{O}$ of snowpack (a) and d -excess values (b) values of the snowpack sampled in the Upper Colorado River
 276 Basin during four different winters along an elevation gradient (Carroll et al., 2021). Regression lines are plotted for
 277 correlations with $p < 0.05$. For each year and for the bulk isotope data over all years, Pearson correlation coefficients (r),
 278 and significant levels (p), as well as slope (b), and intercept (a) of the regression are given. (c) Histogram showing the
 279 distribution of snowpit d -excess values for the sites < 3200 m a.s.l. (“Low elevation”, blue), sites above > 3200 m a.s.l. (“High
 280 elevation”, orange), and groundwater sampled at five wells between 2015 and 2022 (grey, Williams (2023)). The mean d -
 281 excess values for the low and high elevation snowpack (10.7 ‰ and 13.8 ‰, respectively) are significantly different
 282 ($p < 0.0001$, $t = -8.1$) according to the t -test. The mean groundwater d -excess value (10.5 ‰) is not significantly different from
 283 the low elevation snowpack.

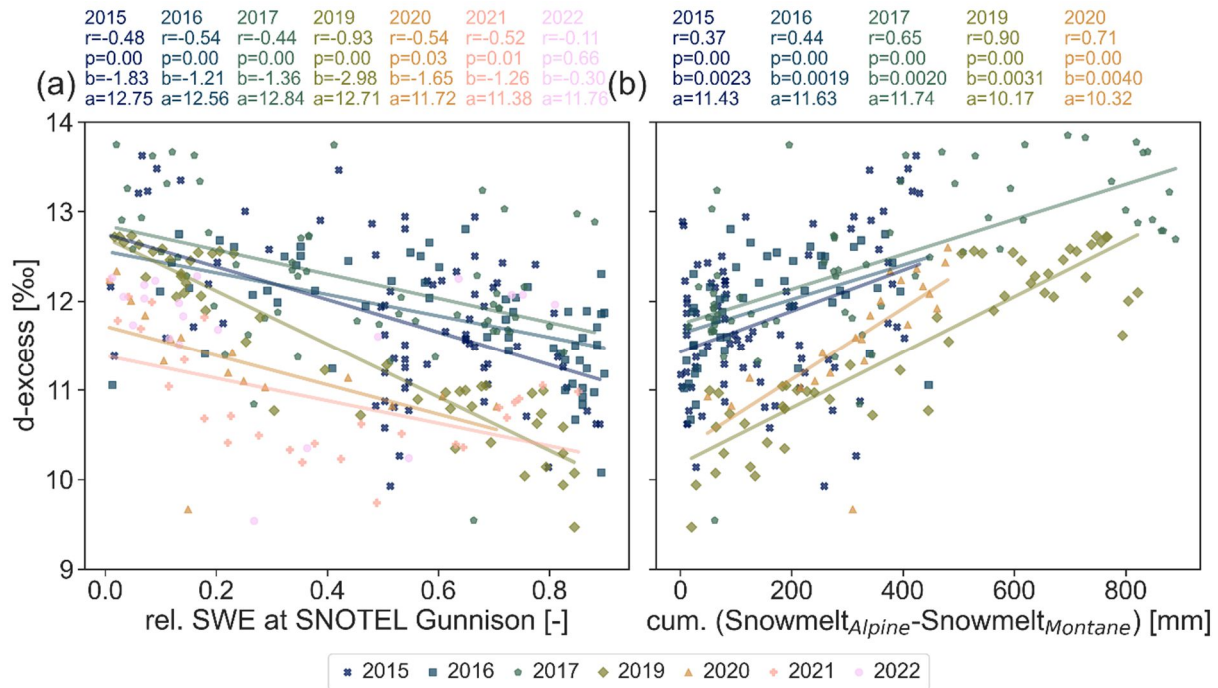
284



285

286 Figure 3 (a) Median annual dynamics of East River streamflow (Q, black, Carroll (2023)) and snow water equivalent (SWE, NWCC (2023)) at the individual SNOTEL sites within the Gunnison River catchment (grey) and the average of all sites (cyan) from water year 2015 to 2022 with semitransparent grey and cyan area representing the standard deviation of Q and SWE, respectively. (b) The $\delta^{18}\text{O}$ (orange) and *d-excess* (red) of all stream water samples collected between water year 2015 and 2022 from the East River at the Pumphouse location (Williams et al., 2023). The orange and red lines are a LOWESS fit to the data points. See Suppl. Fig. 5 for a time series plot of the same data.

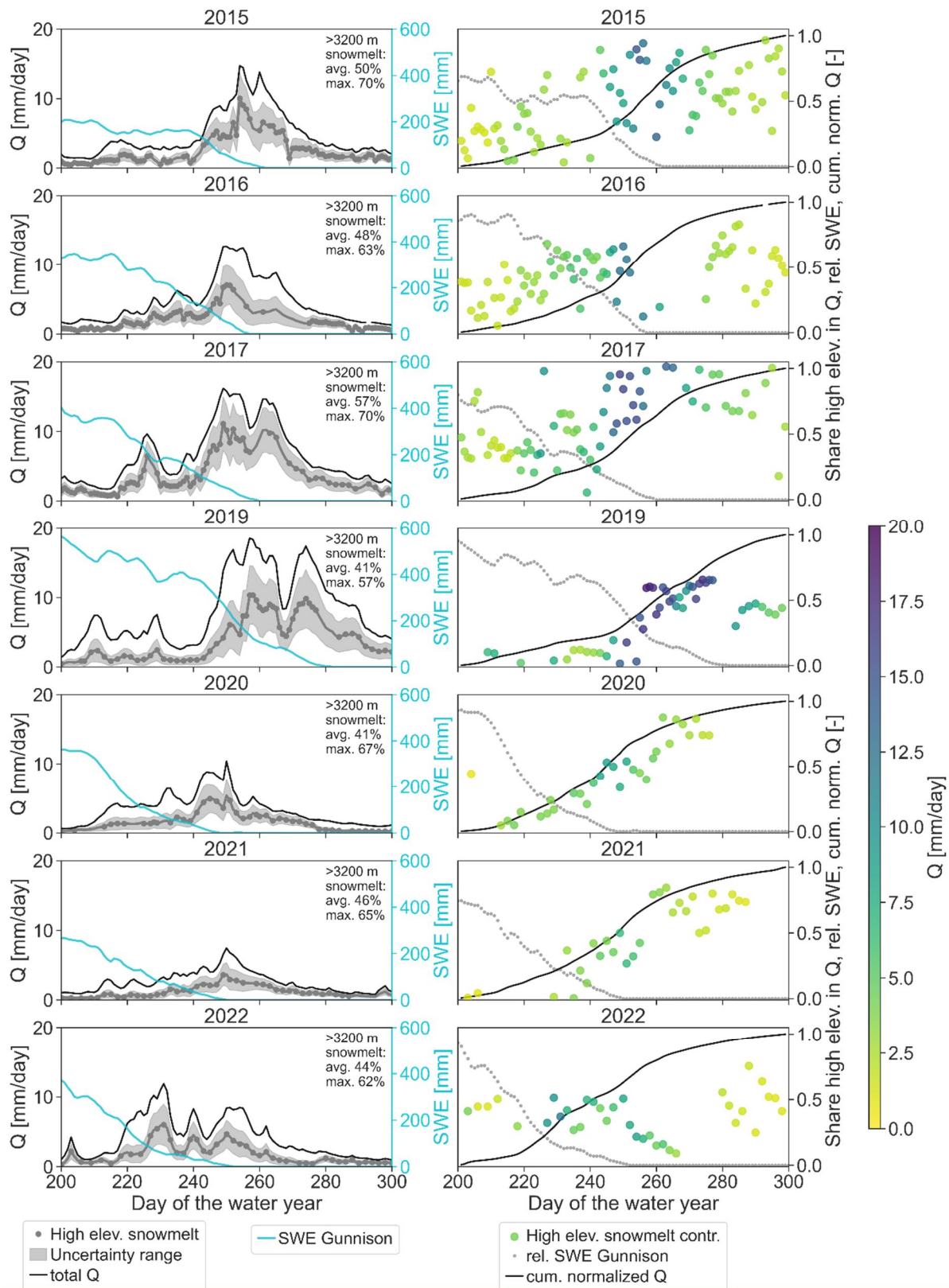
292

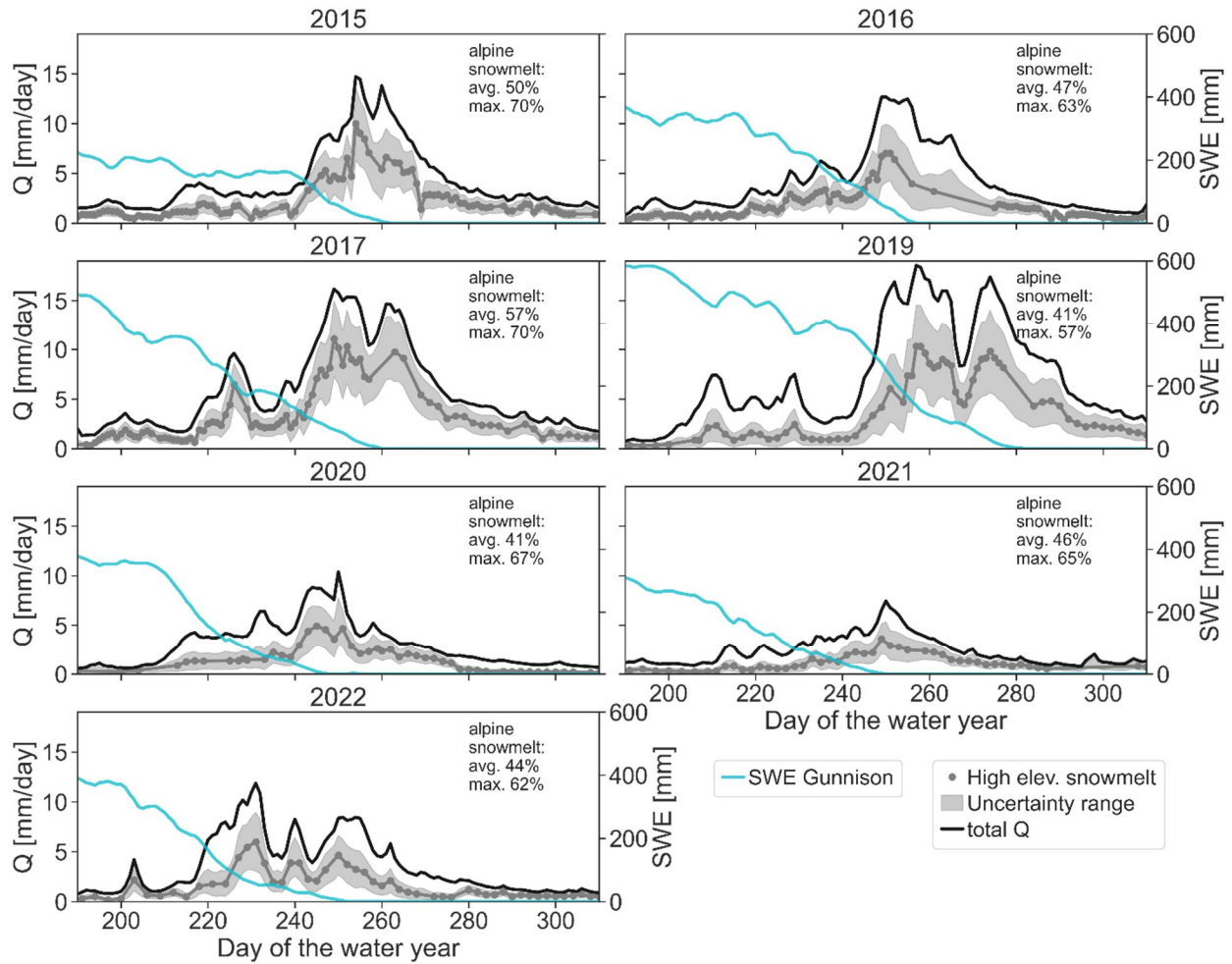


293

294
 295
 296
 297
 298
 299

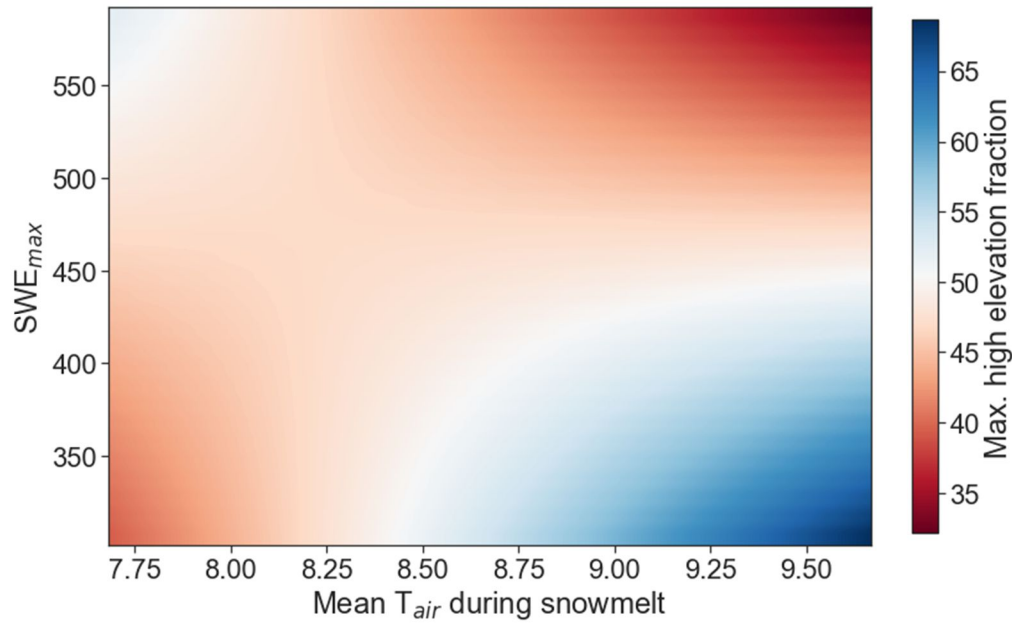
Figure 4 (a) The d -excess of stream water values during snowmelt for seven individual years, shown as a function of relative snow water equivalent (rel. SWE) measured at the SNOTEL stations across the Gunnison River catchment at the time of sampling. For each year, the Pearson correlation (r) and the associated significance level (p) are given as well as the intercept (a) and slope (b) of the regression. (b) The $-d$ -excess of stream water as a function of the cumulative (cum.) differences between the simulated snowmelt at alpine (=highest elevation in the East River) and montane (lowest elevation in the East River) region at the time of each stream water collection. Regression lines are shown for $p \leq 0.05$.



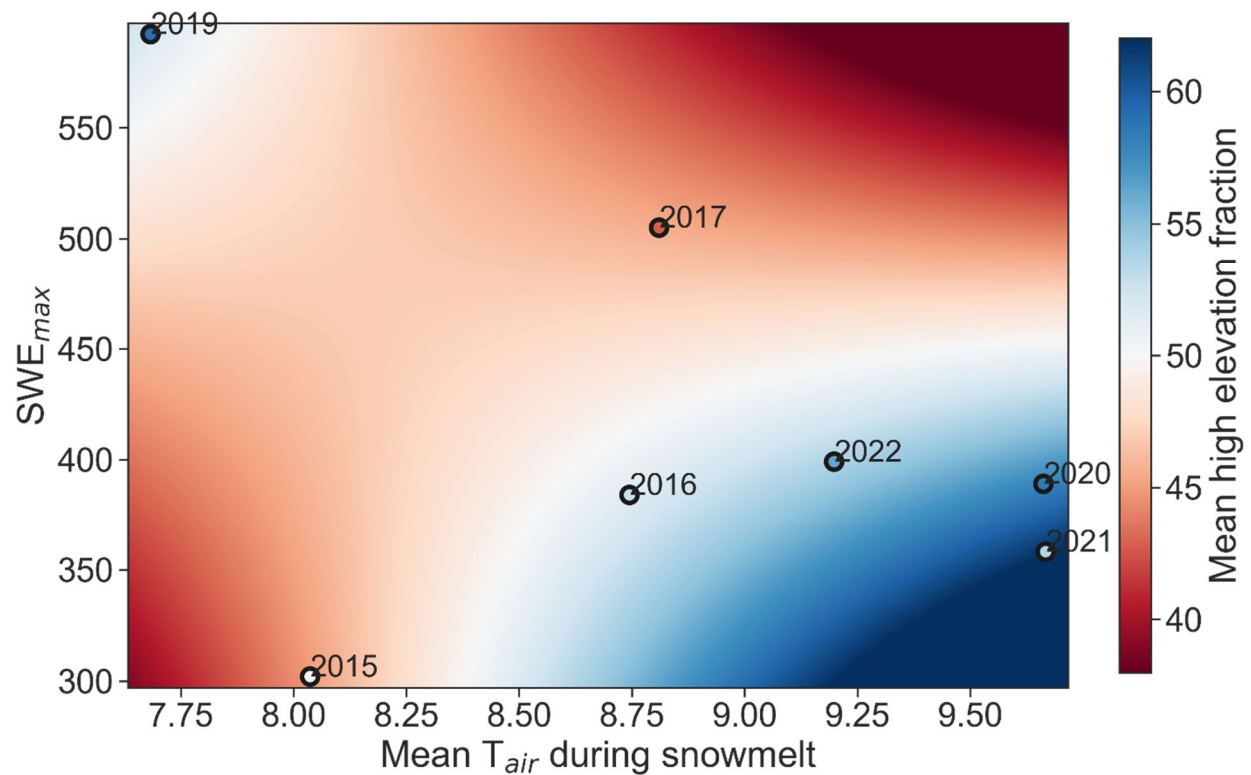


301

302 **Figure 5 (left)** Endmember mixing analyses based on *d-excess* of stream water inferring the share of high elevation snowmelt
 303 (grey dots and lines) in the streamflow during the snowmelt-induced peak flow of the East River. The uncertainty range is
 304 shown as grey bands and it represents the standard deviation (22% on average). **Days 200 and 300 of the water year**
 305 **represent Mid-April and late July, respectively. The cyan line represents the average snow water equivalent (SWE)**
 306 **observed across the SNOTEL sites in Gunnison county. Additionally, we show the total streamflow (Q, black line) as well**
 307 **as the snow water equivalent (SWE, cyan) for the SNOTEL sites in the Gunnison catchment. (right) Share of high elevation**
 308 **snowmelt in the streamflow (points, color coded by Q), relative SWE in Gunnison (1= peak SWE), and cumulative**
 309 **streamflow between day 200 and 300 of the water year. Note that the y axis for the graphs on the right is plotted on the**
 310 **right hand side.**



311

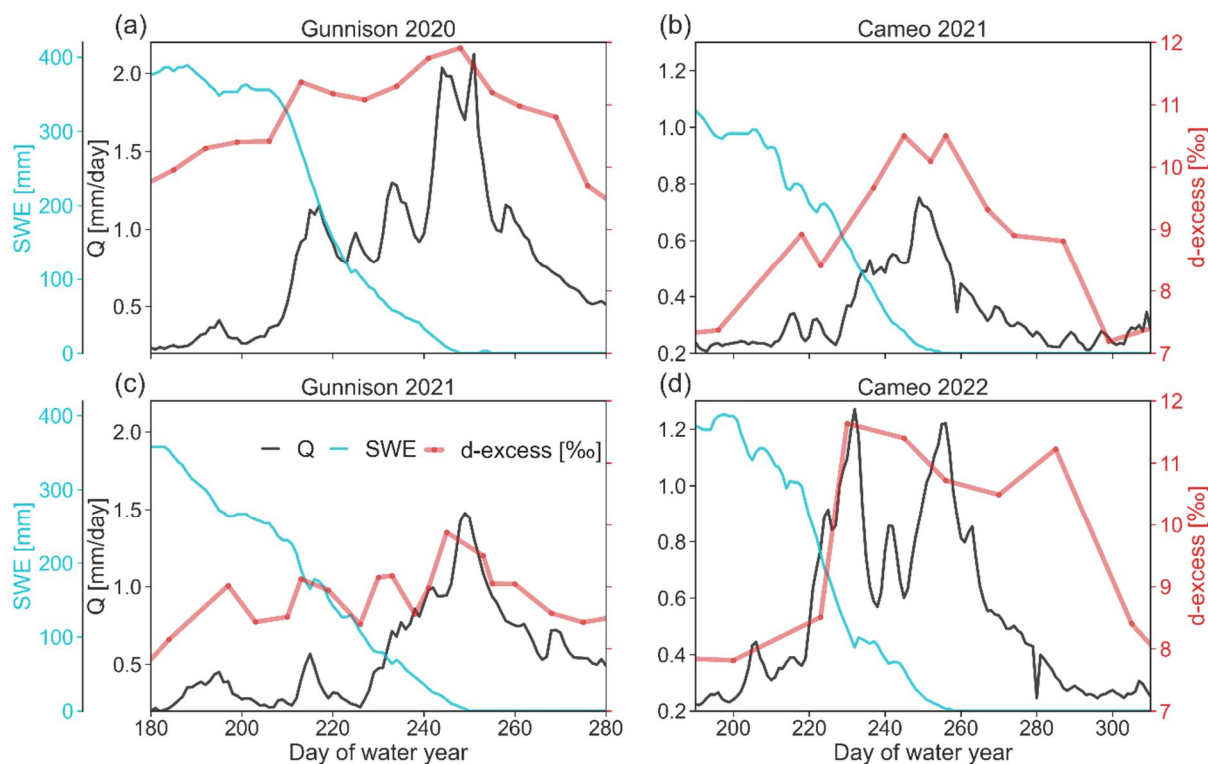


312

313 **Figure 6** Result of the multiple regression analyses to assess predictability of the **maximum-mean** contribution of high
 314 elevation snowmelt to stream water as a function of the maximum snow water equivalent (SWE_{max}) and the air temperature
 315 (T_{air}) during the snowmelt period measured at the SNOTEL sites in Gunnison. Note that the regression includes interaction
 316 between SWE_{max} and T_{air} , as follows: **Maximum high elevation fraction** = $-37.03 * T_{air} - 0.73 * SWE_{max} + 0.089 * T_{air} * SWE_{max} +$
 317 350.74 . **The data points labelled with years indicate the data that went into the model.**

318 **3.2 The *d*-excess dynamics of stream water beyond headwaters**

319 Downstream from the East River, the Gunnison River stream water samples showed similar increase in *d-excess* as
 320 streamflow during the snowmelt season increased. This pattern was observed for both years in which stream water
 321 sampling in Gunnison was done. In 2020, the snowpack was deeper, and the runoff was higher than in 2021.
 322 Additionally, the *d-excess* values of stream water were different for the different years with generally higher values
 323 for 2020 than in 2021 (Figure 7a,c). Despite 30 times larger drainage area of the Gunnison River compared to the East
 324 River, the effect of the high elevation snowmelt on the *d-excess* measurements of stream water was detectable, albeit
 325 dampened given the greater fraction of lower elevations contributing to its flow.
 326 The drainage area of the Colorado River near Cameo is eight times the drainage area of the Gunnison River, but the
 327 difference between the *d-excess* of stream water at the beginning and end of the snowmelt period was greater than 3
 328 % in 2021 and 2022. Thus, despite the large catchment area of the Colorado River near Cameo, and greater mixing
 329 of runoff in reservoirs within that catchment, the snowmelt contribution from high elevation regions was substantial
 330 during the snowmelt peak flow (Figure 7b,d).



331
 332 **Figure 7 Streamflow (Q, black) and *d-excess* (red dots and line) of the stream water before and during snowmelt for the**
 333 **Gunnison River near Gunnison, Colorado in 2020 (a) and 2021 (c) and for the Colorado River near Cameo, Colorado for**
 334 **2021 (b) and 2022 (d). Further shown is the average snow water equivalent (SWE, cyan line) of all the SNOTEL sites located**
 335 **in the Gunnison catchment and in the Colorado River headwaters for the Cameo site, respectively. Note that the y-axes**
 336 **have different scales for each subplot.**

337

338 4 Discussion

339 4.1 The *d-excess* of stream water reflects high elevation snowmelt

340 We find that *d-excess* of stream water can be used to differentiate the effects of snowmelt from low vs. high elevations
341 using three independent approaches: First, the comparisons of *d-excess* dynamics of stream water with the observed
342 snowpack reduction at SNOTEL sites in the region showed a strong relation that was consistent during six of the seven
343 investigated snowmelt periods (Figure 4a). The SNOTEL data do not show an increased snowpack with elevation
344 (Suppl. Fig. 1), but ASO flight data indicate that snowpack depth generally increases with elevation (Carroll, Deems,
345 Sprenger, et al., 2022). Thus, with decreasing SWE during the snowmelt period, the ratio of high elevation snowmelt
346 can increase. Such a trend of relative increase of the high elevation snowpack during low snow years was observed.
347 Second, simulated differences based on spatially explicit hydrological modeling of snowmelt timing and volumes
348 between the montane and alpine regions within the East River catchment correlated significantly with *d-excess* of
349 stream water for every simulated snowmelt period (Figure 4b). Third, the increase in *d-excess* of stream water
350 coincided with the peak streamflow during each snowmelt period (with exception for 2022, Figure 5). Thus, elevated
351 *d-excess* values cannot stem from low elevation snowmelt but most likely result from higher elevation snowmelt as
352 the snowmelt generally progresses from lower to higher elevations due to the temperature gradients across the
353 catchment.

354 Because we observed consistent lapse rates of *d-excess* values in the snowpack during several years (Figure 2b),
355 significant differences between the *d-excess* at lower and higher elevation snowpack (Figure 2c), and also a *d-excess*
356 lapse rate in ~~the~~ winter precipitation (Suppl. Fig. 4), we see a great potential for *d-excess* measurements to serve as a
357 tracer for endmember-mixing analyses to derive high elevation snowmelt contributions to the catchment's streamflow
358 during snowmelt periods.

359 Other studies have also shown that winter precipitation (i.e., snow) snowpack at highest elevations had the highest *d-*
360 *excess* values; monthly weighted precipitation data by Froehlich et al. (2008) indicated a lapse rate for in *d-excess*
361 values of +0.2 ‰/100 m across an elevation range between 469 and 2245 m across in the Alps, and data Data
362 published by Tappa et al. (2016) indicated a lapse rate of +0.6338 ‰/100 m in the Rocky Mountains in Idaho for
363 samples taken between October and May across five sites spanning an elevation gradient from 830 to 1850 m. Rolle
364 (2022) sampled snowpack at ten sites across elevations from 1262 and 1905 m in the Lubrecht Experimental Forest,
365 Greenough, Montana in late March and found a d-excess lapse rate of +0.26 ‰/100 m. Our lapse rate of +0.72 ‰/100
366 m for precipitation and +0.52 ‰/100 m for the snowpack was slightly higher than in the other studies, but we cover a
367 larger elevation gradient and study higher elevations than the other studies. those reported by others. However, the
368 sampling strategies for the different studies are different, and importantly, Nevertheless, the general trend of increased
369 *d-excess* values with elevation was the same for all three-four studies in mountainous systems.

370 However, the processes why we see a d-excess lapse rate in mountain snowfall and snowpack is not yet fully
371 understood. The current literature suggests two potential processes: A

372 One potential explanation for how *d-excess* lapse rates in the snowpack develop is evaporation and sublimation of
373 snow at lower elevation combined with daytime up-valley (anabatic) winds that occur in mountainous areas and the
374 subsequent condensation of the water vapor at colder higher elevation (Beria et al., 2018; Lambán et al., 2015).
375 Sublimation and evaporation from the snowpack leads to kinetic non-equilibrium fractionation that leaves an
376 isotopically enriched snowpack behind (Stichler et al., 2001). Recent in situ stable isotope measurements by Wahl et

377 al. (2021) support this process, because they saw that when radiation driven sublimation outweighed deposition, the
378 vapor was isotopically depleted compared to the snowpack. They further showed that the isotopic composition of the
379 vapor determined the isotopic composition of the humidity flux during deposition conditions (Wahl et al., 2021). For
380 our study region, we have shown previously via spatially explicit snowmelt modeling based on the energy balance
381 and accounting for isotopic fractionation (Carroll et al., 2022a) that the snowpack at lower elevations experience more
382 snow loss to the atmosphere due to higher energy availability than higher elevation, which lead to an elevation gradient
383 of the *d-excess* in the simulations. These simulations also have shown that shading provided by vegetation in forested
384 areas reduces evaporation and sublimation from the underlying snowpack, making *d-excess* values of these snowpack
385 higher than snowpack in non-forested areas at the same elevation (Carroll et al., 2022a). Because the snowpack in
386 forests with higher *d-excess* values melt later than the snowpack in non-forested areas, it also results in an increase in
387 stream water *d-excess* values during the later phase of the snowmelt discharge peak.
388 The second potential explanation for how *d-excess* lapse rates in the snowpack develop would be sub-cloud
389 evaporation, which leads to lower *d-excess* values of precipitation at lower elevations, because the distance between
390 cloud base and ground and the saturation deficit are higher than at higher elevations. Thus, precipitation at lower
391 elevations would experience more kinetic non-equilibrium isotopic fractionation due to evaporation leading to lower
392 *d-excess* (Froehlich et al., 2008). However, this process is less like to occur during winter time and snowfall (Froehlich
393 et al., 2008), and Xing et al. (2023) showed with precipitation and vapor isotope measurements that sub-cloud
394 evaporation altered the *d-excess* values of snowfall much less than rainfall in the Chinese Loess Plateau. While we
395 cannot conclude which process leads to the *d-excess* lapse rate, the observation of a *d-excess* lapse rate in several other
396 high elevation snow studies (Rolle, 2022; Tappa et al., 2016; Froehlich et al., 2008) suggests that we could expect a
397 *d-excess* response due to high elevation snowmelt contributions in the flow of other mountainous streams. Thus, the
398 transferability of our approach to other watersheds will depend on observations of a *d-excess* lapse rate in the
399 snowpack, which will likely be influenced by climatic conditions that lead to thick a snowpack without mid-winter
400 melt, relatively steady moisture source of the snowfall, and accessibility to sample the snowpack near peak SWE.
401 Importantly, Our long-term sampling of the precipitation in the East River can ~~further~~ rule out a potential
402 precipitation *d-excess* seasonality to influence the *d-excess* of stream water during the snowmelt period (Suppl. Fig.
403 3). Therefore, there are several independent data sources that all point towards high elevation snowmelt contributions
404 to the catchment streamflow driving the observed *d-excess* of stream water variation during the snowmelt period.
405 Our findings, based on endmember-mixing analyses via *d-excess* values highlight the importance of high elevation
406 snowpack for runoff generation. Since the *d-excess* values in the groundwater are more similar to the lower elevation
407 snowpack (Figure 2c), we infer that groundwater recharge is dominated by early snowmelt in relatively lower
408 elevations infiltrating into a relatively dry subsurface. High elevation snowmelt occurs during later freshet when the
409 soils are already saturated or near saturation, which leads to fast runoff generation and thus shorter travel times and
410 higher runoff efficiency (as outlined by Webb et al., 2022) of high elevation snowmelt than low elevation snowmelt.
411 This temporal aspect of the high elevation snowmelt and its larger contribution to streamflow later in the snowmelt
412 hydrograph is reflected in the endmember mixing results that show the highest share on the recession limb of the
413 hydrograph (Suppl. Fig. 6). The interannual variation in *d-excess* of stream water and the derived high elevation

414 snowmelt contributions indicate that the snowpack of the upper subalpine and alpine region could be most important
415 in years of relatively low snowpack accumulation and comparably high spring air temperatures. The observed
416 regression stems from the generally higher volume share of high elevation snowpack compared to low elevation
417 snowpack during low snow years, and the faster melt out during warmer spring temperatures, both leading to larger
418 contributions of high elevation snowmelt to the spring hydrograph peak. Thus, with the projection of a reduced
419 snowpack in the western United States (Siirila-Woodburn et al., 2021), understanding the high elevation snowpack
420 dynamics could most likely become more important, and *d-excess* observations are a tool to investigate the timing
421 (e.g., trend towards earlier melt) and fate (e.g., streamflow contribution vs. sublimation or groundwater recharge) of
422 the snowpack throughout the melting period.

423 **4.2 Limitations and opportunities of *d-excess* of stream water with scale**

424 Our results show that the *d-excess* patterns of stream water observed in a headwater stream can be upscaled because
425 we see a similar *d-excess* pattern of stream water at larger scales from stream water sampling ~~in~~ at the USGS
426 streamgages of the Gunnison near Gunnison and Colorado River near Cameo. The latter sampling site is an entirely
427 different catchment to the north of East River and Gunnison River in which the snowpack was not sampled for its *d-*
428 *excess* values. However, the *d-excess* signal of stream water for Coal Creek, a smaller headwater catchment to the
429 west of the East River catchment, did not show a similar pattern (Suppl. Fig. 8, Suppl. Fig. 9), likely because of a
430 lower representation of high elevation bands within in the catchment (Suppl. Fig. 10). Twenty nine percent of the Coal
431 Creek catchment area is the upper subalpine region, but only 6% of the catchment is alpine (>3500 m). Thus, high
432 elevation snowpack with the highest *d-excess* values is essentially missing in Coal Creek, which presumably
433 dampened *d-excess* response of stream water. We therefore hypothesize that the applicability of the *d-excess* of stream
434 water as a signal for high elevation snowmelt is dependent on a sufficient area with high elevation (>3200 m) and
435 sufficient elevation gradient in the catchment of the sampled stream. Lastly, although we see *d-excess* dynamics of
436 stream water in response to high elevation snowmelt at relatively large scales, the isotope dynamics may likely not be
437 detectable downstream from large reservoirs. Initial sampling of the Colorado River near the Colorado-Utah state line
438 with a drainage area of 46,230 km² that includes several large reservoirs indicates that stream water *d-excess* changes
439 are rather dampened and might not hold sufficient information to infer high elevation snowmelt contributions (not
440 shown).

441 Because snowpack volumes are getting lower, and snowmelt is starting earlier in mountainous regions due to climate
442 change (Musselman et al., 2021), we ~~need-could benefit by~~ finding ways to assess the effect of these both at sub-
443 annual to decadal time scales. Short term identification of a snow drought could allow for adaptive water management
444 measures on the sub-annual time scale, whereas long-term trends might show the trajectory of mountain snow
445 dynamics. With 0.2 ‰ measurement uncertainty of the *d-excess* values due to 0.025 ‰ and 0.1 ‰ precision (1 σ) in
446 $\delta^{18}\text{O}$ and $\delta^2\text{H}$, respectively, the observed variation of *d-excess* in snowpack and stream water are at least ten times
447 larger. Our results and the discussion in the previous section show that measurements of *d-excess* of stream water is a
448 relatively ~~most effective~~ efficient way to obtain catchment integrated information about the high elevation snowpack.
449 Although SNOTEL sites are point measurements and therefore do not represent integrated patterns across
450 heterogeneous mountainous regions, *d-excess* of stream water does integrate throughout catchment areas. The lidar

451 based ASO data provide spatially explicit snowpack observations on catchment scales, but such data collection ~~is can~~
452 ~~be difficult~~ and represents only snapshots in time, although time series changes of snowpack during the
453 snowmelt period might be more informative. The ~~costs~~ difficulty of large-scale flight-based data collection may also
454 make monitoring of interannual SWE changes difficult to conduct over every basin where trends induced by climate
455 change ~~need to~~ may be useful to identify. The *d-excess* application introduced in this study ~~is can be efficient~~
456 ~~effective~~, applicable across scales that vary by orders of magnitude, and ~~needs~~ uses limited labor and instruments ~~and~~
457 ~~investments~~ for the water sampling (e.g., autosampler) and standardized laboratory analyses (e.g., laser spectrometer).
458 ~~We suggest that~~ The *d-excess* of stream water could serve as ~~an~~ complementary information source in addition to the
459 currently applied streamflow shape and flashiness at low and high flows to derive relations between snow persistence
460 effects on the hydrograph across different climates (Le et al., 2022).

461 Measurements of *d-excess* of stream water ~~can~~ could further help disentangle ~~ing~~ rapid high elevation snowmelt
462 contributions to the streamflow versus groundwater inflow to the stream. This ~~could be highly beneficial~~ is important
463 because mountainous catchments with lower groundwater influence were found to be more sensitive to snowpack
464 changes due to warming (Tague and Grant, 2009).

465 5 Conclusion

466 Our snowpack and stream water stable hydrogen and oxygen isotope sampling program during several years links *d-*
467 *excess* of stream water at the catchment outlet to high elevation snowmelt contributions during the snowmelt period.
468 The relation between *d-excess* of stream water and snowmelt dynamics at high elevations was consistent during several
469 years. End member mixing analyses based on *d-excess* values quantified the temporal dynamics of high elevation
470 snowmelt contributions and its relative importance for the runoff generation from mountainous catchments. As
471 compared to other approaches, such catchment integrated information ~~is~~ may be an ~~cost~~-effective way to better
472 quantify the role of upper subalpine and alpine snowpack for streamflow contributions in snow-dominated
473 mountainous systems. Our findings indicate that high elevation snowpack contributions to the streamflow tend to be
474 more important for runoff generation during years with lower snowpack and warmer spring temperatures. Thus, the
475 high elevation snowpack could likely play a bigger role in the coming decades as snowpack reduces and air
476 temperature rise.

477 Because we observed an increase of *d-excess* in the stream water during snowmelt for catchments of 85 to over 20,000
478 km² in size, the *d-excess* appears to be a robust tracer across a wide range of drainage basin scales. We ~~hypothesize~~
479 suggest though that transferability of this approach could depend on the share of high elevation regions of the
480 catchment area ~~to that~~ contribute to streamflow, the presence of a *d-excess* lapse rate in the snowpack, and the absence
481 of large reservoirs upstream from the isotope sampling location. With increasing availability of stable isotope data of
482 mountainous catchments across the globe, future synthesis work could investigate the role of high elevation snowmelt
483 contributions in headwater regions worldwide.

484 Data availability

485 The data on East River streamflow (Carroll et al., 2023) (~~Newcomer et al., 2022~~), snowpack (Carroll et al., 2021), as
486 well as stable isotopes of precipitation, groundwater, and ~~stable isotopes of~~ stream water (Williams et al., 2023) are

487 available online as cited. Snow water equivalent data from the SNOTEL sites are made available by NWCC (2023) ~~at~~
488 <https://wcc.sc.egov.usda.gov/reportGenerator/>, streamflow and water stable hydrogen and oxygen isotope data from
489 the Gunnison near Gunnison and the Colorado River near Cameo sites are available from USGS National Water
490 Information System (USGS, 2023) ~~(NWIS; <https://doi.org/10.5066/F7P55KJN>)~~ database.

491 **Code availability**

492 The HydroMix code by Beria et al. (2019) is available on GitHub at
493 https://github.com/harshberia93/HydroMix/tree/20191007_GMD (last access: 20 August 2023).

494 **Acknowledgements**

495 This work was supported by the US Department of Energy Office of Science under contract DE-AC02-05CH11231
496 as part of Lawrence Berkeley National Laboratory Watershed Function Science Focus Area. We would like to express
497 appreciation to the Rocky Mountain Biological Laboratory for handling Forest Service permitting. We thank Jarral
498 Ryter in the WCU Western Colorado University Chemistry program for analytical help with Cavity Ring-Down
499 Spectroscopy. Any use of trade, firm, or product names is for descriptive purposes only and does not imply
500 endorsement by the U.S. Government.

501 **Author contributions**

502 MS conducted the data analysis and wrote the initial draft of the manuscript. All co-authors contributed either to the
503 analyses, the database, and the interpretation of both as well as improving the manuscript.

504 **Competing interests**

505 The authors declare that they have no conflict of interest.

506 **Competing interests**

507 The authors declare no competing interests.

508 **References**

509 Bennett, K. E. and Talsma, C.: Concurrent Changes in Extreme Hydroclimate Events in the Colorado River Basin,
510 *Water*, 13, 978, <https://doi.org/10.3390/w13070978>, 2021.

511 Beria, H., Larsen, J. R., Ceperley, N. C., Michelon, A., Vennemann, T., and Schaepli, B.: Understanding snow
512 hydrological processes through the lens of stable water isotopes, *Wiley Interdiscip. Rev. Water*, 5, e1311,
513 <https://doi.org/10.1002/wat2.1311>, 2018.

514 Beria, H., Larsen, J. R., Michelon, A., Ceperley, N. C., and Schaepli, B.: HydroMix v1.0: a new Bayesian mixing
515 framework for attributing uncertain hydrological sources, *Geosci. Model Dev.*, 13, 2433–2450,
516 <https://doi.org/10.5194/gmd-13-2433-2020>, 2020.

517 Bureau of Reclamation: Colorado River Basin Water Supply and Demand Study Executive Summary, Reclam.
518 Manag. Water West, 2012.

519 Carroll, R. W. H., Deems, J. S., Niswonger, R., Schumer, R., and Williams, K. H.: The Importance of Interflow to
520 Groundwater Recharge in a Snowmelt-Dominated Headwater Basin, *Geophys. Res. Lett.*, 46, 5899–5908,
521 <https://doi.org/10.1029/2019GL082447>, 2019.

522 Carroll, R. W. H., Manning, A. H., Niswonger, R., Marchetti, D., and Williams, K. H.: Baseflow Age Distributions
523 and Depth of Active Groundwater Flow in a Snow-Dominated Mountain Headwater Basin, *Water Resour. Res.*, 56,
524 e2020WR028161, <https://doi.org/10.1029/2020WR028161>, 2020.

525 Carroll, R. W. H., Brown, W., Newman, A., Beutler, C., and Williams, K. H.: East River Watershed Stable Water
526 Isotope Data in Precipitation, Snowpack and Snowmelt 2016-2020, ESS-DIVE Repos.,
527 <https://doi.org/10.15485/1824223>, 2021.

528 Carroll, R. W. H., Deems, J., Sprenger, M., Maxwell, R., Brown, W., Newman, A., Beutler, C., and Williams, K. H.:
529 Modeling Snow Dynamics and Stable Water Isotopes Across Mountain Landscapes, *Geophys. Res. Lett.*, 49,
530 e2022GL098780, <https://doi.org/10.1029/2022GL098780>, 2022a.

531 Carroll, R. W. H., Deems, J., Maxwell, R., Sprenger, M., Brown, W., Newman, A., Beutler, C., Bill, M., Hubbard, S.
532 S., and Williams, K. H.: Variability in observed stable water isotopes in snowpack across a mountainous watershed in
533 Colorado, *Hydrol. Process.*, 36, e14653, <https://doi.org/10.1002/hyp.14653>, 2022b.

534 Carroll, R. W. H., Newman, A., Beutler, C., Williams, K., and O’Ryan, D.: Stream discharge and temperature data
535 collected within the East River, Colorado for the Lawrence Berkeley National Laboratory Watershed Function Science
536 Focus Area (water years 2019 to 2022), ESS-DIVE Repos., <https://doi.org/10.15485/1779721>, 2023.

537 Craig, H.: Isotopic variations in meteoric waters, *Science*, 133, 1702–1703,
538 <https://doi.org/10.1126/science.133.3465.1702>, 1961a.

539 Craig, H.: Standard for Reporting Concentrations of Deuterium and Oxygen-18 in Natural Waters, *Science*, 133,
540 1833–1834, <https://doi.org/10.1126/science.133.3467.1833>, 1961b.

541 Dansgaard, W.: Stable isotopes in precipitation, *Tellus*, 16, 436–468, <https://doi.org/10.1111/j.2153-3490.1964.tb00181.x>, 1964.

543 Dozier, J., Bair, E. H., and Davis, R. E.: Estimating the spatial distribution of snow water equivalent in the world’s
544 mountains, *WIREs Water*, 3, 461–474, <https://doi.org/10.1002/wat2.1140>, 2016.

545 Fassnacht, S. R., Dressler, K. A., and Bales, R. C.: Snow water equivalent interpolation for the Colorado River Basin
546 from snow telemetry (SNOTEL) data, *Water Resour. Res.*, 39, <https://doi.org/10.1029/2002WR001512>, 2003.

547 Faybishenko, B., Arora, B., Dwivedi, D., and Brodie, E.: Statistical framework to assess long-term spatio-temporal
548 climate changes: East River mountainous watershed case study, *Stoch. Environ. Res. Risk Assess.*,
549 <https://doi.org/10.1007/s00477-022-02327-7>, 2022.

550 Freudiger, D., Kohn, I., Seibert, J., Stahl, K., and Weiler, M.: Snow redistribution for the hydrological modeling of
551 alpine catchments, *Wiley Interdiscip. Rev. Water*, 4, e1232, <https://doi.org/10.1002/wat2.1232>, 2017.

552 Froehlich, K., Kralik, M., Papesch, W., Rank, D., Scheifinger, H., and Stichler, W.: Deuterium excess in precipitation
553 of Alpine regions - Moisture recycling, *Isotopes Environ. Health Stud.*, 44, 61–70,
554 <https://doi.org/10.1080/10256010801887208>, 2008.

555 Gaskill, D. L., Mutschler, F. E., and Kramer, J. H.: Geologic map of the Gothic Quadrangle, Gunnison County,
556 Colorado, <https://doi.org/10.3133/gq1689>, 1991.

557 Gat, J. R.: Atmospheric water balance-the isotopic perspective, *Hydrol. Process.*, 14, 1357–1369,
558 [https://doi.org/10.1002/1099-1085\(20000615\)14:8<1357::AID-HYP986>3.0.CO;2-7](https://doi.org/10.1002/1099-1085(20000615)14:8<1357::AID-HYP986>3.0.CO;2-7), 2000.

- 559 Hammond, J. C., Sexstone, G. A., Putman, A. L., Barnhart, T. B., Rey, D. M., Driscoll, J. M., Liston, G. E., Rasmussen,
560 K. L., McGrath, D., Fassnacht, S. R., and Kampf, S. K.: High Resolution SnowModel Simulations Reveal Future
561 Elevation-Dependent Snow Loss and Earlier, Flashier Surface Water Input for the Upper Colorado River Basin, *Earths*
562 *Future*, 11, e2022EF003092, <https://doi.org/10.1029/2022EF003092>, 2023.
- 563 Hoerling, M., Barsugli, J., Livneh, B., Eischeid, J., Quan, X., and Badger, A.: Causes for the century-long decline in
564 Colorado river flow, *J. Clim.*, 32, 8181–8203, <https://doi.org/10.1175/JCLI-D-19-0207.1>, 2019.
- 565 Hubbard, S. S., Williams, K. H., Agarwal, D., Banfield, J., Beller, H., Bouskill, N., Brodie, E., Carroll, R., Dafflon,
566 B., Dwivedi, D., Falco, N., Faybishenko, B., Maxwell, R., Nico, P., Steefel, C., Steltzer, H., Tokunaga, T., Tran, P.
567 A., Wainwright, H., and Varadharajan, C.: The East River, Colorado, Watershed: A Mountainous Community Testbed
568 for Improving Predictive Understanding of Multiscale Hydrological–Biogeochemical Dynamics, *Vadose Zone J.*, 17,
569 180061, <https://doi.org/10.2136/vzj2018.03.0061>, 2018.
- 570 Immerzeel, W. W., Lutz, A. F., Andrade, M., Bahl, A., Biemans, H., Bolch, T., Hyde, S., Brumby, S., Davies, B. J.,
571 Elmore, A. C., Emmer, A., Feng, M., Fernández, A., Haritashya, U., Kargel, J. S., Koppes, M., Kraaijenbrink, P. D.
572 A., Kulkarni, A. V., Mayewski, P. A., Pacheco, P., Painter, T. H., Pellicciotti, F., Rajaram, H., Rupper, S., Sinisalo,
573 A., Shrestha, A. B., Viviroli, D., Wada, Y., Xiao, C., Yao, T., and Baillie, J. E. M.: Importance and vulnerability of
574 the world ' s water towers, *Nature*, 577, <https://doi.org/10.1038/s41586-019-1822-y>, 2020.
- 575 Kendall, C. and McDonnell, J. J.: *Isotope tracers in catchment hydrology*, Elsevier, Amsterdam, Netherlands, 839 pp.,
576 1998.
- 577 Lambán, L. J., Jódar, J., Custodio, E., Soler, A., Sapriza, G., and Soto, R.: Isotopic and hydrogeochemical
578 characterization of high-altitude karst aquifers in complex geological settings. The Ordesa and Monte Perdido
579 National Park (Northern Spain) case study, *Sci. Total Environ.*, 506–507, 466–479,
580 <https://doi.org/10.1016/j.scitotenv.2014.11.030>, 2015.
- 581 Le, E., Ameli, A., Janssen, J., and Hammond, J.: Snow Persistence Explains Stream High Flow and Low Flow
582 Signatures with Differing Relationships by Aridity and Climatic Seasonality, *Hydrol. Earth Syst. Sci. Discuss.*, 1–22,
583 <https://doi.org/10.5194/hess-2022-106>, 2022.
- 584 Marchetti, D. W. and Marchetti, S. B.: Stable isotope compositions of precipitation from Gunnison, Colorado 2007–
585 2016: implications for the climatology of a high-elevation valley, *Heliyon*, 5, e02120,
586 <https://doi.org/10.1016/j.heliyon.2019.e02120>, 2019.
- 587 Musselman, K. N., Addor, N., Vano, J. A., and Molotch, N. P.: Winter melt trends portend widespread declines in
588 snow water resources, *Nat. Clim. Change*, 11, 418–424, <https://doi.org/10.1038/s41558-021-01014-9>, 2021.
- 589 NWCC: SNOTEL, <https://wcc.sc.gov.usda.gov/reportGenerator/>, 2023.
- 590 Painter, T. H., Berisford, D. F., Boardman, J. W., Bormann, K. J., Deems, J. S., Gehrke, F., Hedrick, A., Joyce, M.,
591 Laidlaw, R., Marks, D., Mattmann, C., McGurk, B., Ramirez, P., Richardson, M., Skiles, S. M. K., Seidel, F. C., and
592 Winstal, A.: The Airborne Snow Observatory: Fusion of scanning lidar, imaging spectrometer, and physically-based
593 modeling for mapping snow water equivalent and snow albedo, *Remote Sens. Environ.*, 184, 139–152,
594 <https://doi.org/10.1016/j.rse.2016.06.018>, 2016.
- 595 Rodhe, A.: Spring Flood Meltwater or Groundwater?: Paper presented at the Nordic Hydrological Conference
596 (Vemdalen, Sweden, August, 1980), *Hydrol. Res.*, 12, 21–30, <https://doi.org/10.2166/nh.1981.0002>, 1981.
- 597 Rolle, J.: Determining Spatial Controls on Snow Isotopic Signature and Tracing the Snowmelt Pulse as it Moves
598 Through Two Montane Tracing the Snowmelt Pulse as it Moves Through Two Montane Catchments Catchments,
599 Graduate Student Thesis, The University Of Montana, 2022.

600 Rozanski, K., Araguás-Araguás, L., and Gonfiantini, R.: Isotopic patterns in modern global precipitation, in: *Climate*
601 *Change in Continental Isotopic Records*, vol. 78, edited by: Swart, P. K., Lohmann, K. C., McKenzie, J., and Savin,
602 S., American Geophysical Union, Washington, D. C., 1–36, <https://doi.org/10.1029/GM078p0001>, 1993.

603 Schneider, D. and Molotch, N. P.: Real-time estimation of snow water equivalent in the Upper Colorado River Basin
604 using MODIS-based SWE Reconstructions and SNOTEL data, *Water Resour. Res.*, 52, 7892–7910,
605 <https://doi.org/10.1002/2016WR019067>, 2016.

606 Siirila-Woodburn, E. R., Rhoades, A. M., Szinai, J., Tague, C., Nico, P. S., and Huning, L. S.: A low-to-no snow
607 future and its impacts on water resources in the western United States, *Nat. Rev. Earth Environ.*, 2, 800–819,
608 <https://doi.org/10.1038/s43017-021-00219-y>, 2021.

609 Sprenger, M., Carroll, R. W. H., Denny-frank, J., Siirila-woodburn, E. R., Newcomer, M. E., Brown, W., and
610 Williams, K. H.: Variability of Snow and Rainfall Partitioning Into Evapotranspiration and Summer Runoff Across
611 Nine Mountainous Catchments, *Geophys. Res. Lett.*, 49, e2022GL099324, <https://doi.org/10.1029/2022GL099324>,
612 2022.

613 Stichler, W., Schotterer, U., Fröhlich, K., Ginot, P., Kull, C., Gäggeler, H., and Pouyaud, B.: Influence of sublimation
614 on stable isotope records recovered from high-altitude glaciers in the tropical Andes, *J. Geophys. Res. Atmospheres*,
615 106, 22613–22620, <https://doi.org/10.1029/2001JD900179>, 2001.

616 Stock, B. C., Jackson, A. L., Ward, E. J., Parnell, A. C., Phillips, D. L., and Semmens, B. X.: Analyzing mixing
617 systems using a new generation of Bayesian tracer mixing models, *PeerJ*, 6, e5096, <https://doi.org/10.7717/peerj.5096>,
618 2018.

619 Tague, C. and Grant, G. E.: Groundwater dynamics mediate low-flow response to global warming in snow-dominated
620 alpine regions, *Water Resour. Res.*, 45, <https://doi.org/10.1029/2008WR007179>, 2009.

621 Tappa, D. J., Kohn, M. J., McNamara, J. P., Benner, S. G., and Flores, A. N.: Isotopic composition of precipitation in
622 a topographically steep, seasonally snow-dominated watershed and implications of variations from the Global
623 Meteoric Water Line, *Hydrol. Process.*, 30, 4582–4592, <https://doi.org/10.1002/hyp.10940>, 2016.

624 USGS: USGS Water Data for the Nation, <https://doi.org/10.5066/F7P55KJN>, 2023.

625 Wahl, S., Steen-Larsen, H. C., Reuder, J., and Hörhold, M.: Quantifying the Stable Water Isotopologue Exchange
626 Between the Snow Surface and Lower Atmosphere by Direct Flux Measurements, *J. Geophys. Res. Atmospheres*,
627 126, 1–24, <https://doi.org/10.1029/2020JD034400>, 2021.

628 Webb, R. W., Musselman, K. N., Ciafone, S., Hale, K. E., and Molotch, N. P.: Extending the vadose zone:
629 Characterizing the role of snow for liquid water storage and transmission in streamflow generation, *Hydrol. Process.*,
630 36, e14541, <https://doi.org/10.1002/hyp.14541>, 2022.

631 Williams, K. H., Beutler, C. A., Bill, M., Brown, W., Newman, A. W., and Versteeg, R.: Stable Water Isotope Data
632 for the East River Watershed, Colorado (2014-2023), ESS-DIVE Repos., <https://doi.org/10.15485/1668053>, 2023.

633 Xing, M., Liu, W., Hu, J., and Wang, Z.: A set of methods to evaluate the below-cloud evaporation effect on local
634 precipitation isotopic composition: a case study for Xi'an, China, *Atmospheric Chem. Phys.*, 23, 9123–9136,
635 <https://doi.org/10.5194/acp-23-9123-2023>, 2023.

636

637

642 **Stream water sourcing from high elevation snowpack inferred from**
643 **stable isotopes of water: A novel application of *d*-excess values**

644 Matthias Sprenger^{1*}, Rosemary W.H. Carroll², David Marchetti³, Carl Bern⁴, Wendy Brown⁵, Alexander Newman⁵,
645 Curtis Beutler⁵, Kenneth H. Williams^{1,5}

646 ¹Lawrence Berkeley National Laboratory, Berkeley, CA, USA

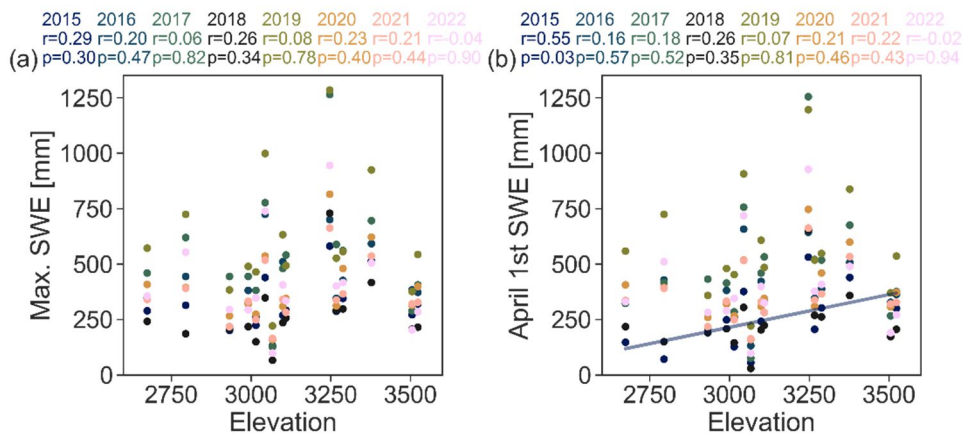
647 ²Desert Research Institute, Reno, NV, USA

648 ³Western Colorado University, Gunnison, CO, USA

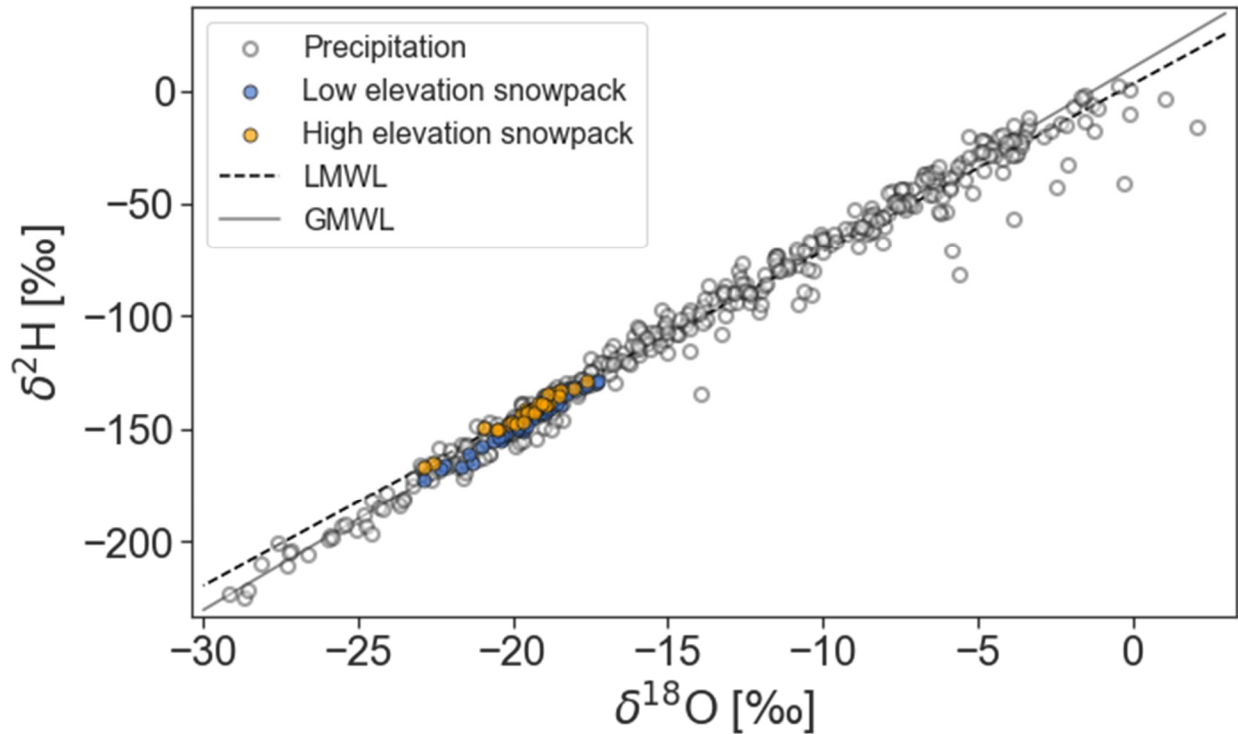
649 ⁴U.S. Geological Survey, Denver, CO, USA

650 ⁵Department of Environmental Systems Science, ETH Zurich, Zurich, Switzerland⁶Rocky Mountain Biological
651 Laboratory, Crested Butte, CO, USA

652 *Corresponding author: msprenger@lbl.gov

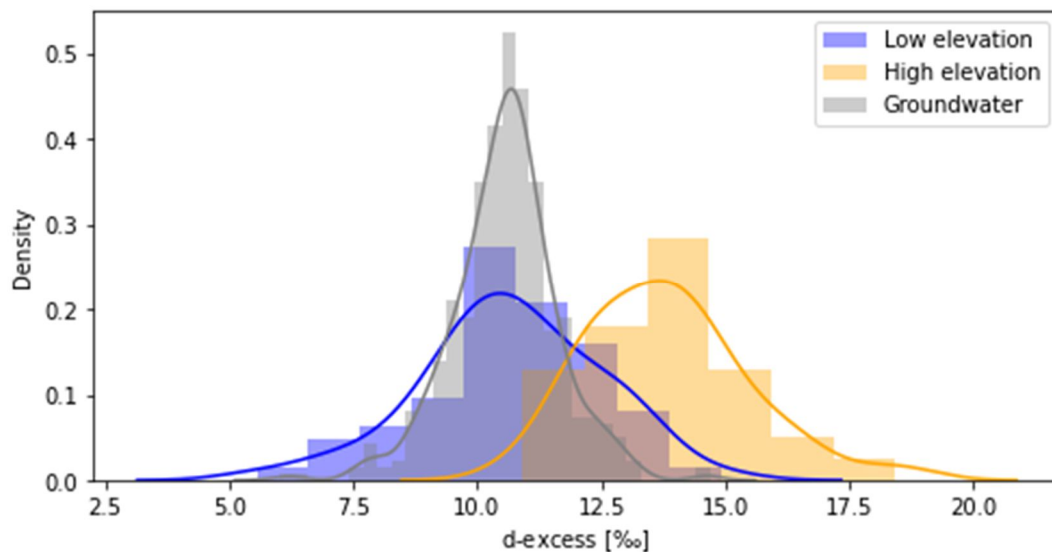


654 **Suppl. Fig. 1 (a) Relation between maximum snow water equivalent (SWE) at the 15 SNOTEL sites in the Gunnison River**
655 **basin and the elevation of the SNOTEL sites for the years 2015 to 2022. (b) same as in (a), but with SWE on April 1st. Given**
656 **are the Pearson correlation coefficients for each year and the years are color coded (data from NWCC, 2023).**



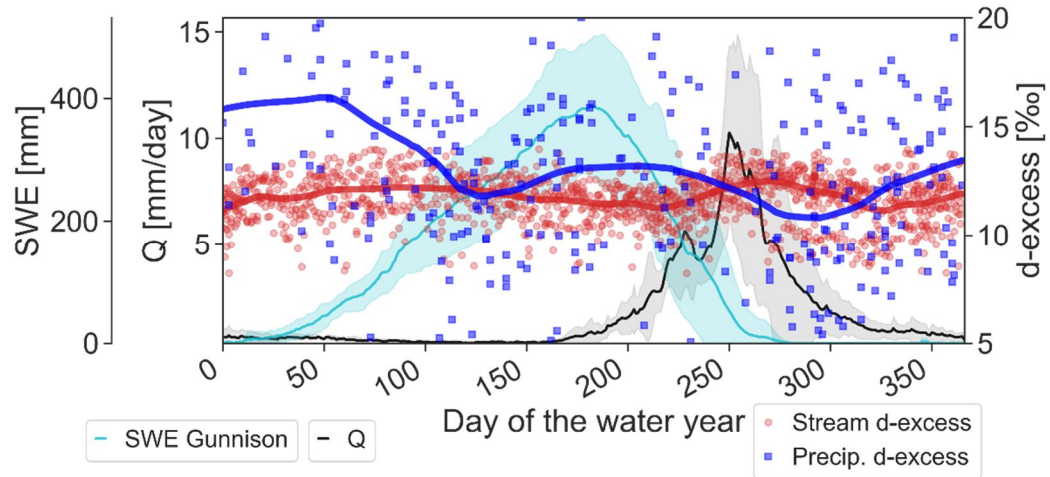
657

658 Suppl. Fig. 2 Precipitation samples from 2015 to 2022 (white points) and snowpack sampled at sites <3200 m a.s.l. (“Low
 659 elevation”, blue) and sites above >3200 m a.s.l. (“High elevation”, orange). Also shown are the Global Meteoric Water Line
 660 (GMWL: $\delta^2\text{H} = 8.2 \delta^{18}\text{O} + 11.27$, Rozanski et al. (1993)) and the Local Meteoric Water Line (LMWL: $\delta^2\text{H} = 7.4$
 661 $\delta^{18}\text{O} + 2.4$, Carroll et al. (2022b)).



662

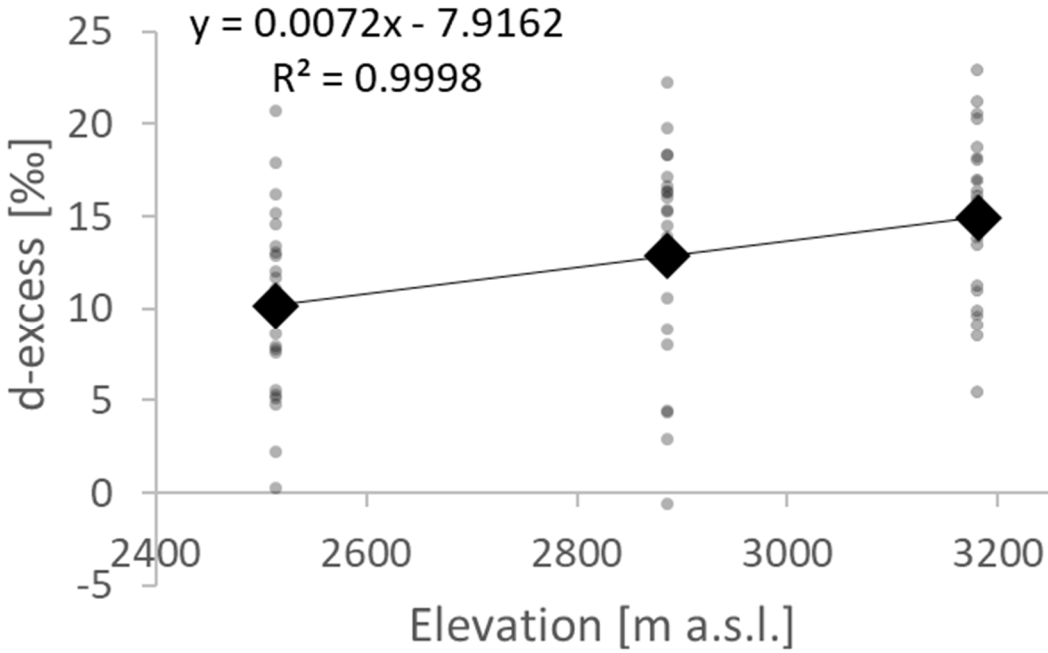
663 Suppl. Fig. 3 Histogram showing the distribution of snowpit d-excess for the sites <3200 m a.s.l. (“Low elevation”, blue),
 664 sites above >3200 m a.s.l. (“High elevation”, orange), and groundwater sampled at five wells between 2015 and 2022 (grey).
 665 The mean values for the low and high elevation snowpack (10.7 ‰ and 13.8 ‰, respectively) are significantly different
 666 ($p < 0.0001$, $t = -8.1$) according to the t-test. The mean groundwater d-excess (10.5 ‰) is not significantly different from the
 667 low elevation snowpack.



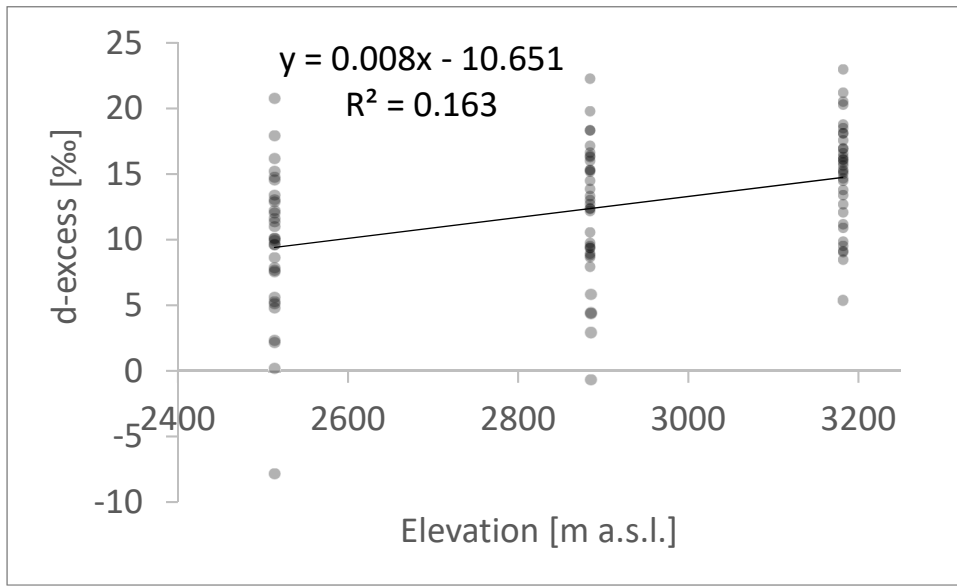
668

669 **Suppl. Fig. 3** Median annual dynamics of snow water equivalent (SWE) at the Gunnison SNOTEL stations (cyan) and East
 670 River streamflow (Q, black) from water year 2015 to 2022 with semitransparent area representing the range. The d-excess
 671 of all stream water at East River (red) and precipitation (blue) samples collected between water year 2015 and 2022. The
 672 red and blue lines represent a lowess filter to show any trends in the data.

673



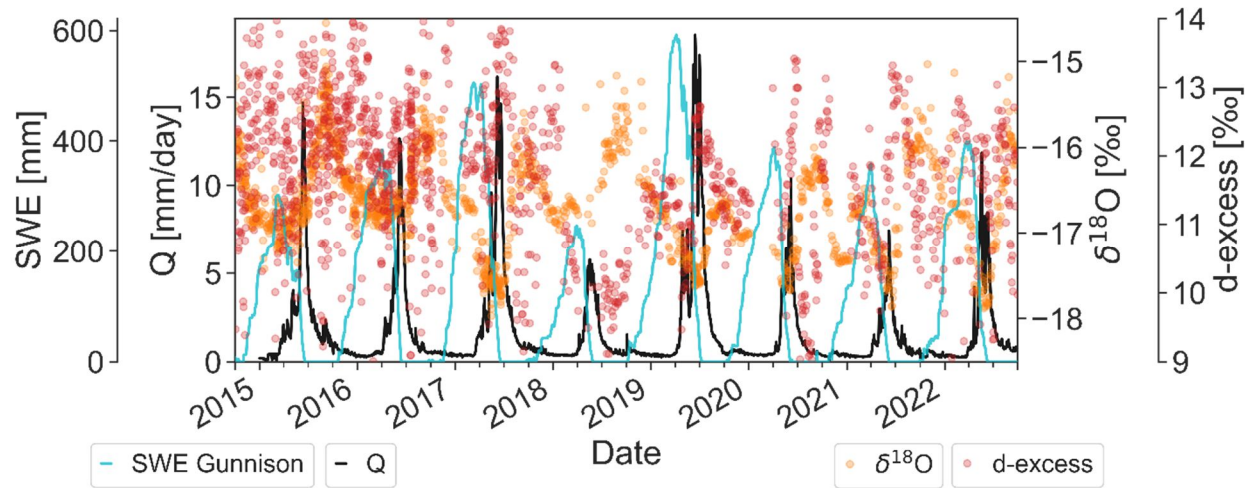
674



675

676 **Suppl. Fig. 4** The d-excess of winter precipitation from samples collected between November and April during the water
 677 years 2021 and 2022 at the locations Estess (2513 m), Mount Crested Butte (2885 m) and Irwin Barn (3181 m). The black
 678 diamonds show the mean values and half-transparent dots are individual samples. The regression line shows the d-excess
 679 lapse rate of 0.7 ‰/100 m.

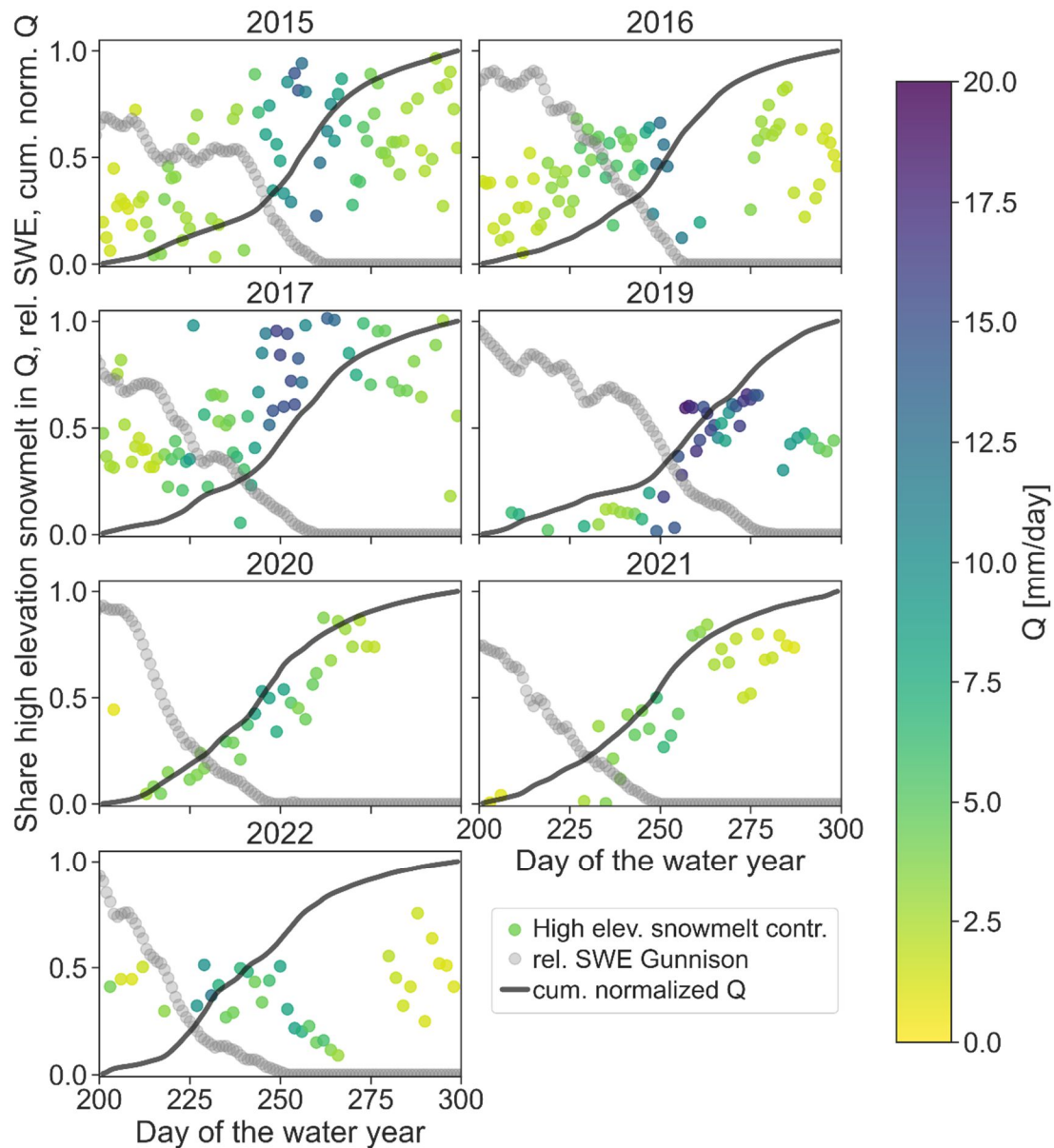
680



681

682
683
684

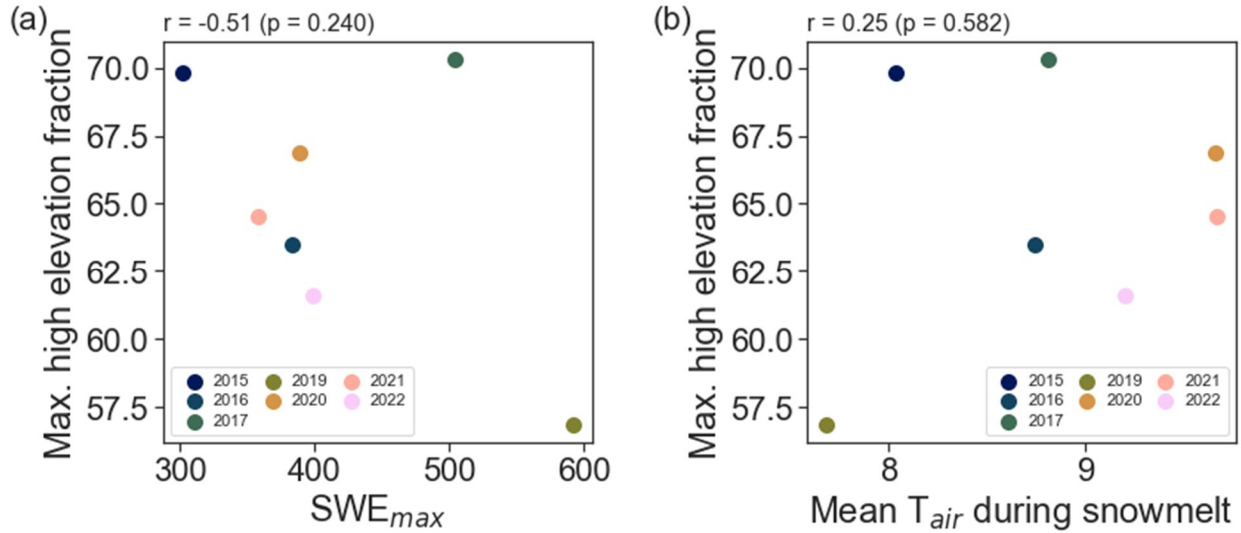
Suppl. Fig. 5 Snow water equivalent (SWE) at the Gunnison SNOTEL stations (cyan line), streamflow (Q, black line) at the East River, as well as the $\delta^{18}\text{O}$ (orange points) and *d-excess* (red points) of the stream water sampled at Pumphouse for the water years 2015 to 2022.



685

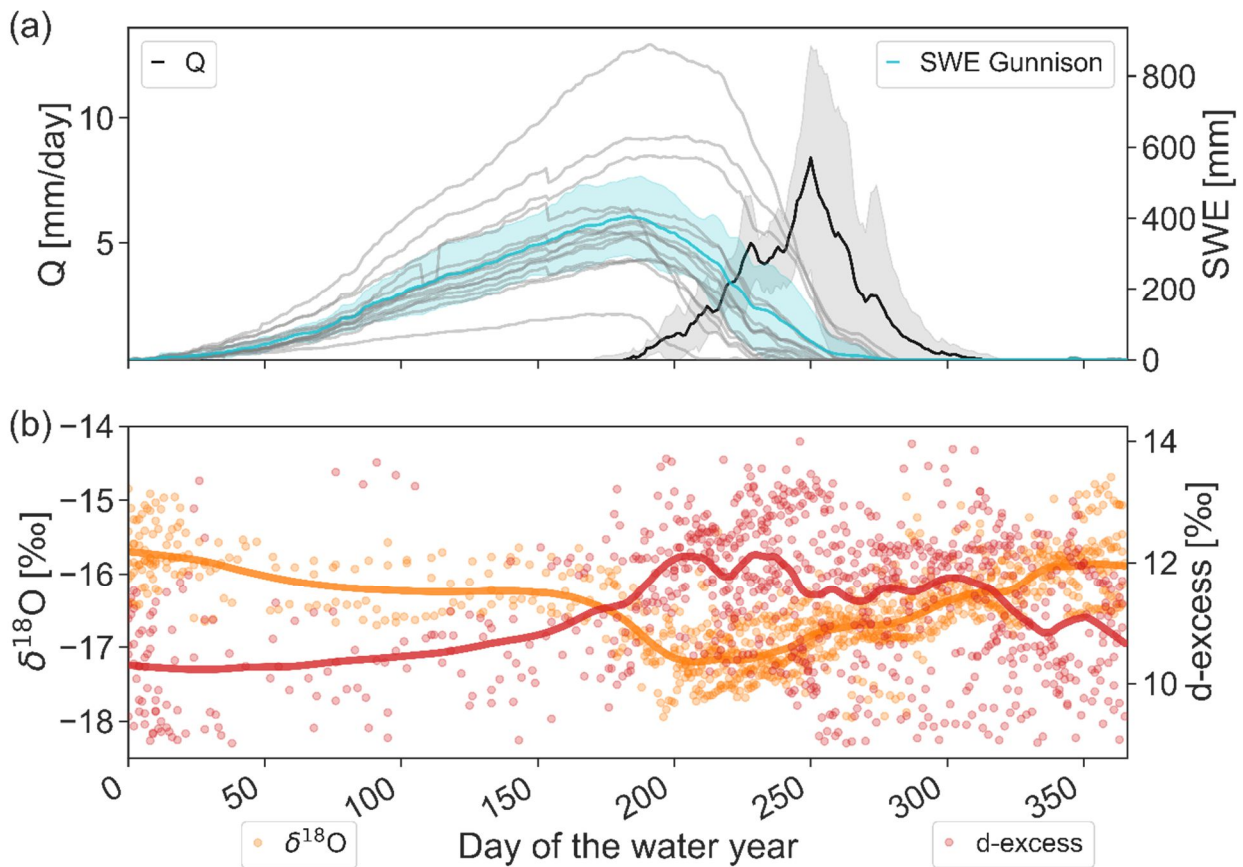
686 **Suppl. Fig. 6** Additionally, we show the **T**otal streamflow (Q, black line) as well as the snow water equivalent (SWE, cyan)
 687 for the SNOTEL sites in the Gunnison catchment. (right) Share of high elevation snowmelt in the streamflow (points, color
 688 coded by Q), relative **observed** SWE in Gunnison (1= **peak maximum** SWE), and cumulative streamflow between day 200
 689 and 300 of the water year. Note that the y-axis for the graphs on the right is plotted on the right-hand side.

690



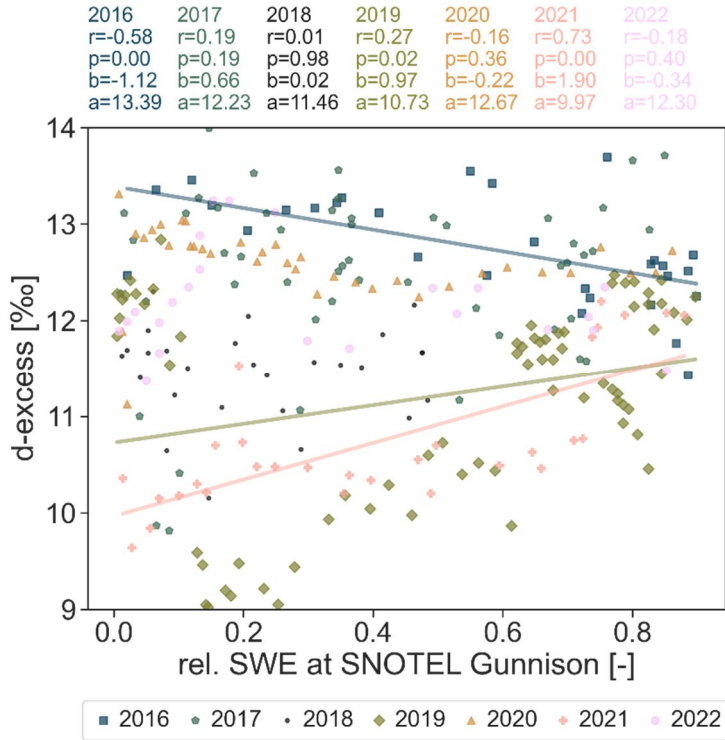
691

692 **Suppl. Fig. 7** Relation between maximum fraction of high elevation snowpack contributions to the snowmelt runoff and the
 693 maximum snow water equivalent (in a) and mean air temperature during the snowmelt period (in b).



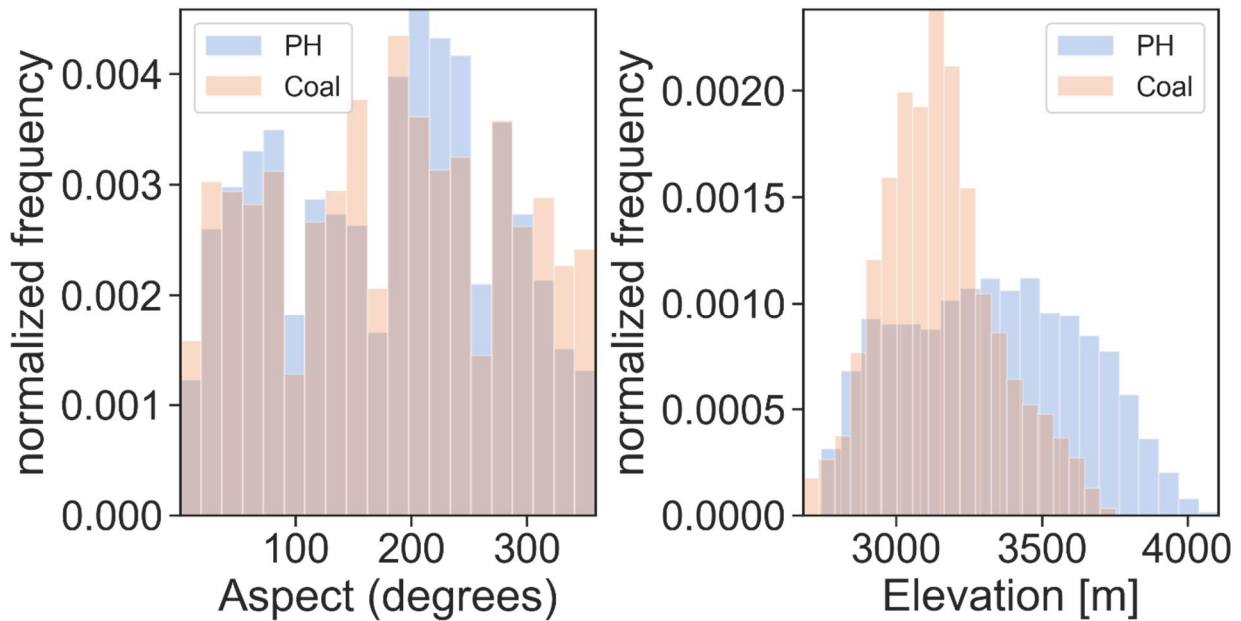
694

695 **Suppl. Fig. 8** (a) Median annual dynamics of Coal Creek streamflow (Q , black) and snow water equivalent (SWE) at the
 696 individual SNOTEL sites within the Gunnison River catchment (grey) and the average of all sites (cyan) from water year
 697 2016 to 2022 with semitransparent grey and cyan area representing the standard deviation of Q and SWE, respectively. (b)
 698 The $\delta^{18}\text{O}$ (orange) and d -excess (red) of all stream water samples collected between water year 2016 and 2022 from the East
 699 River at the Pumhouse location. The orange and red lines are a LOWESS fit to the data points.



700

701 **Suppl. Fig. 9** The *d-excess* of Coal Creek stream water during snowmelt for seven individual years, shown as a function of
 702 relative SWE measured at the SNOTEL stations across the Gunnison River catchment at the time of sampling. For each
 703 year, the Pearson correlation (r) and the associated significance level (p) are given as well as the intercept (a) and slope (b)
 704 of the regression.



705

706 **Suppl. Fig. 10** Distribution of aspect (left) and elevation (right) across the East River catchment defined at Pumphouse (PH,
 707 blue) and Coal Creek (Coal, orange).

708 Suppl. Table 1 SNOTEL sites located in the Gunnison River Basin (~~data from~~(data from NWCC, 2023)
 709 <https://wcc.sc.egov.usda.gov/reportGenerator/>).

Station Id	Station Name	Elevation (m)	Latitude	Longitude	County Name
380	Butte	3108.96	38.8944	-106.95	Gunnison
1059	Cochetopa Pass	3066.59	38.1627	-106.6	Saguache
409	Columbine Pass	2795.32	38.4182	-108.38	Montrose
538	Idarado	2990.7	37.9339	-107.68	Ouray
618	Mc Clure Pass	2674.32	39.129	-107.29	Gunnison
622	Mesa Lakes	3099.21	39.0574	-108.06	Mesa
675	Overland Res.	3015.39	39.0904	-107.64	Delta
680	Park Cone	2932.48	38.8198	-106.59	Gunnison
682	Park Reservoir	3044.04	39.0443	-107.88	Delta
701	Porphyry Creek	3288.18	38.4886	-106.34	Gunnison
713	Red Mountain Pass	3377.18	37.8917	-107.71	San Juan
1128	Sargents Mesa	3504.9	38.2856	-106.37	Saguache
737	Schofield Pass	3247.03	39.0147	-107.05	Gunnison
762	Slumgullion	3523.49	37.9908	-107.2	Hinsdale
1141	Upper Taylor	3266.54	38.9907	-106.75	Gunnison

710

711

Station Id	Station Name	Elevation (m)	Latitude	Longitude	County Name
1030	Arapaho Ridge	3345.48	40.351	-106.38	Grand
1061	Bear River	2777.34	40.0615	-107.01	Routt
1041	Beaver Ck Village	2610.61	39.5987	-106.51	Eagle
335	Berthoud Summit	3448.51	39.8036	-105.78	Grand
345	Bison Lake	3341.83	39.7646	-107.36	Garfield
913	Buffalo Park	2819.1	40.2284	-106.6	Grand
1101	Chapman Tunnel	3078.48	39.2621	-106.63	Pitkin
408	Columbine	2794.1	40.3959	-106.6	Jackson
415	Copper Mountain	3207.41	39.4892	-106.17	Summit
1120	Elliot Ridge	3215.34	39.8638	-106.42	Summit
485	Fremont Pass	3452.16	39.3801	-106.2	Summit
505	Grizzly Peak	3395.17	39.6465	-105.87	Summit
542	Independence Pass	3230.27	39.0754	-106.61	Pitkin
547	Ivanhoe	3212.9	39.2923	-106.55	Pitkin
970	Jones Pass	3177.84	39.7645	-105.91	Grand
556	Kiln	2933.4	39.3172	-106.62	Pitkin
565	Lake Irene	3255.87	40.4145	-105.82	Grand
607	Lynx Pass	2718.51	40.0783	-106.67	Routt
618	Mc Clure Pass	2674.32	39.129	-107.29	Gunnison

1040	Mccoys Park	2900.48	39.6023	-106.54	Eagle
622	Mesa Lakes	3099.21	39.0574	-108.06	Mesa
1014	Middle Fork Camp	2733.75	39.7957	-106.03	Grand
658	Nast Lake	2661.21	39.297	-106.61	Pitkin
669	North Lost Trail	2809.95	39.0782	-107.14	Gunnison
675	Overland Res.	3015.39	39.0904	-107.64	Delta
682	Park Reservoir	3044.04	39.0443	-107.88	Delta
688	Phantom Valley	2756.92	40.398	-105.85	Grand
737	Schofield Pass	3247.03	39.0147	-107.05	Gunnison
802	Summit Ranch	2856.28	39.718	-106.16	Summit
842	Vail Mountain	3142.49	39.6177	-106.38	Eagle
869	Willow Creek Pass	2902.61	40.3473	-106.1	Grand

712

713 Any use of trade, firm, or product names is for descriptive purposes only and does not imply endorsement by the U.S.

714 Government.